


Technical Report No. 224

036040-19-T

THE THEORY OF SIGNAL DETECTABILITY: CYCLO-STATIONARY
PROCESSES IN ADDITIVE NOISE

by

J. R. Lapointe, Jr.

Approved by: 
Theodore G. Birdsall

for

COOLEY ELECTRONICS LABORATORY

Department of Electrical and Computer Engineering
The University of Michigan
Ann Arbor, Michigan

Contract No. N00014-67-A-0181-0032
Office of Naval Research
Department of the Navy
Arlington, Virginia 22217

October 1973

Approved for public release; distribution unlimited.

ABSTRACT

Cyclo-Stationary (CS) processes are those nonstationary processes that appear to be stationary when observed at integral multiples of a basic interval. Wide Sense Cyclo-Stationary (WSCS) processes possess autocorrelation functions and autocorrelation matrices with a cyclic structure for continuous and discrete time respectively. Discrete time WSCS processes normally arise from sampling continuous time WSCS processes. Other sampling schemes such as multiplexing samples from different stationary random processes or multiplexing samples from the sensors of an array also generate random processes with a cyclic structure in the autocorrelation matrix.

The optimum detector for the fixed time forced choice detection of discrete time WSCS processes in additive noise is designed according to the likelihood ratio. The detector design is constrained to preserving the cyclic structure of the signal autocorrelation matrix followed by a signal enhancement filter followed by energy detection. The structure of the signal enhancement filter is clearly identifiable with the cyclic structure of the signal autocorrelation matrix. A suboptimum detector is also presented and is the low input signal-to-noise ratio form of the optimum detector.

The optimum and suboptimum detector performance is evaluated for a discrete time real zero mean CS Gauss-Markov process in the region $0.01 \leq P_D \leq 0.99$ and $0.01 \leq P_{FA} \leq 0.9$. The optimum and suboptimum Receiver Operating Characteristics (ROC) are binormal in this region. There is little difference between the optimum and suboptimum performance though the suboptimum ROC is more binormal than the optimum ROC.

FOREWORD

Detection of the existence of some sort of periodic structure in a reception is the motivation for this research. The research is theoretical and deals with the techniques of defining the problem and establishing its mathematical solution. Of primary importance to the theoretician is the realization that the vector form of the problem is the same as that of a point-sensor antenna array. Thus the rich field of array processing can be tapped for formal solutions.

The type of periodicity investigated is a common physical occurrence, but its formal description is obtuse enough that it has not been a subject of detection theory previously. The physical picture involves a periodic mechanism that produces a turbulence or other random process. The periodicity of the generator is then hidden in the process as a cyclo-stationary characteristic: if sampled at the period, the samples are stationary, but if sampled at a multiple of the period, the sample statistics depend on the local position within a period.

This research establishes a foundation for applied research in the detection and analysis of cyclo-stationary processes.

TABLE OF CONTENTS

	<u>Page</u>
ABSTRACT	iii
FOREWORD	v
LIST OF ILLUSTRATIONS	x
LIST OF APPENDICES	xii
LIST OF SYMBOLS	xiii
CHAPTER I: INTRODUCTION	1
1.1 Basic Problem	1
1.2 Cyclo-Stationary Processes	1
1.2.1 Continuous Parameter Cyclo-Stationary Processes	2
1.2.2 Discrete Parameter Cyclo-Stationary Processes	4
1.2.3 Cyclic Structure of the Auto-correlation Matrix	5
1.3 Generation of Cyclo-Stationary Processes	9
1.3.1 Continuous Parameter Cyclo-Stationary Processes	9
1.3.2 Discrete Parameter Cyclo-Stationary Processes	9
1.3.2.1 Sampling Continuous Parameter Cyclo-Stationary Processes	10
1.3.2.2 Sampling Continuous Parameter Stationary Random Processes	10
1.4 Procedure	11
1.5 Historical Background	12
1.6 Organization of this Study	13
1.7 Notation	13

TABLE OF CONTENTS (Cont.)

	<u>Page</u>
CHAPTER II: BACKGROUND	15
2.1 Review of Detection Theory	15
2.1.1 Detector Design	16
2.1.2 Detector Evaluation	18
2.1.3 Normal ROC	20
2.1.4 Binormal ROC	22
2.2 Performance Evaluation and Characteristic Functions	24
CHAPTER III: OPTIMUM DETECTOR FOR WIDE SENSE CYCLO-STATIONARY PROCESSES	27
3.1 Introduction	27
3.2 Detector Design	27
3.2.1 The Sufficient Statistic and Three Common Interpretations	28
3.2.2 Expansion of the Sufficient Statistic	33
3.3 Detector Description	35
3.4 Summary	37
CHAPTER IV: PERFORMANCE EVALUATION OF THE OPTIMUM DETECTOR	39
4.1 Introduction	39
4.2 Model Description	39
4.2.1 Noise Model	39
4.2.2 Signal Model	39
4.3 Evaluation Procedures	42
4.3.1 ROC Generation	43
4.3.2 Input Signal-to-Noise Ratio	45
4.3.3 Detectability Index	46
4.4 Performance	48
4.5 Summary	61
CHAPTER V: A SUBOPTIMUM DETECTOR	62
5.1 Introduction	62
5.2 Suboptimum Detector	62
5.3 Evaluation Procedures	64
5.4 Performance	65

TABLE OF CONTENTS (Cont.)

	<u>Page</u>
5.4.1 Decision Variable Statistics	66
5.4.2 ROC Comparison	69
5.5 Summary	74
CHAPTER VI: CONCLUSIONS	75
6.1 Summary and Conclusions	75
6.2 Contributions	78
6.3 Suggestions for Future Work	79
REFERENCES	102
DISTRIBUTION LIST	105

LIST OF ILLUSTRATIONS

<u>Figure</u>	<u>Title</u>	<u>Page</u>
2.1	Illustration of the basic signal detection problem	15
2.2	Normal ROC's with detectability index d'	21
2.3	Binormal ROC's with detectability index d'_e and slope SLOPE	23
3.1	Triangularization	30
3.2	Simultaneous diagonalization	31
3.3	Estimator-correlator	32
3.4	Optimum detector for WSCS processes	43
4.1	ROC curves for optimum detector for $K = 4, P = 4, \rho_s = 0.25$	49
4.2	ROC curves for optimum detector for $K = 16, P = 4, \rho_3 = 0.25$	50
4.3	ROC curves for optimum detector for $K = 64, P = 4, \rho_s = 0.25$	51
4.4	ROC curves for optimum detector for $K = 1, P = 16, \rho_s = 0.707$	52
4.5	ROC curves for optimum detector for $K = 4, P = 16, \rho_s = 0.707$	53
4.6	ROC curves for optimum detector for $K = 16, P = 16, \rho_s = 0.707$	54
4.7	Performance summary of the optimum detector as a function of d'_e for $\rho_s = 0.707$	57
4.8	Performance summary of the optimum detector as a function of SNR_I for $P = 16$	58

LIST OF ILLUSTRATIONS (Cont.)

<u>Figure</u>	<u>Title</u>	<u>Page</u>
4.9	P as a function of SNR_I for $\rho_s = 0.707$	59
5.1	A suboptimum detector for WSCS processes	63
5.2	Behavior of the terms in the expressions for the mean and variance of the optimum and suboptimum decision variables under H_0 and H_1	68
5.3	Performance summary of the suboptimum detector as a function of d_{es} for $\rho_s = 0.707$	72
5.4	Performance summary of the suboptimum detector as a function of SNR_I for $P = 16$	73
5.5	Comparison of optimum and suboptimum detectability indexes for $\rho_s = 0.707$ and $P = 16$	73

LIST OF TABLES

<u>Table</u>	<u>Title</u>	<u>Page</u>
4.1	Summary of optimum detector performance	56
5.1	Summary of suboptimum detector performance	71

LIST OF APPENDICES

	<u>Page</u>
APPENDIX A: Simultaneous Diagonalization	81
APPENDIX B: Realizability	88
APPENDIX C: Parameters of the Binormal ROC	89
APPENDIX D: Eigenvalues and Input Signal-to-Noise Ratios	93
APPENDIX E: Example of Factorizing the Auto-correlation Matrix of a WSCS Process	95

LIST OF SYMBOLS

<u>Symbol</u>	<u>Definition</u>
A	$P \times P$ modulation autocorrelation matrix
A_{nm}	$P \times P$ crosscorrelation matrices
C	$KP \times KP$ lower triangular carrier matrix, $T = C^*C$
CS	cyclo-stationary
d'	detectability index for a normal ROC
d_e'	detectability index of optimum detector
d_{es}'	detectability index of suboptimum detector
E	signal energy
$E\{\cdot\}$	expected value operator
f_0	carrier frequency in hertz
$f[\cdot H_0]$	probability density function under H_0
$f[\cdot H_1]$	probability density function under H_1
$g(t)$	elementary waveform
H	linear filter that produces \hat{S} from Y
H_0	noise alone hypothesis
H_1	signal and noise hypothesis
I_p	$P \times P$ identity matrix
K	a non-zero integer indicating the number of periods in a CS process
$L[\cdot]$	likelihood ratio, $L[\cdot] = [\cdot H_1] / [\cdot H_0]$
M	$P \times P$ lower triangular modulation matrix, $A = M^*M$

LIST OF SYMBOLS (Cont.)

<u>Symbol</u>	<u>Definition</u>
M_K	$KP \times KP$ diagonal matrix with M repeated along the diagonal
m_0	mean of the decision variable under H_0
m_1	mean of the decision variable under H_1
N	noise random process
$N(B, D)$	normal multivariate probability distribution with vector mean B and autocorrelation matrix D
N_0	noise power per hertz
P	a non-zero integer called the period indicating the number of elements in the period of a CS process
P_D	probability of detection
P_{FA}	probability of false alarm
Q	matrix of eigenvectors
ROC	receiver operating characteristic
R_N	autocorrelation matrix of the noise N
$r_N(n)$	diagonal elements of R_N
R_S	autocorrelation matrix of the CS process S
$r_S(n)$	diagonal elements of R_S
$r_S(n, m)$	elements of R_S
$R_S(t_1, t_2)$	autocorrelation function of the CS process $s(t)$
$R_x(\tau)$	autocorrelation function of $x(t)$
S	discrete parameter cyclo-stationary process
\hat{S}	minimum mean-square estimate of S , $\hat{S} = HY$

LIST OF SYMBOLS (Cont.)

<u>Symbol</u>	<u>Definition</u>
SLOPE	slope of the optimum ROC
SLOPE _s	slope of the suboptimum ROC
SNR _I	input signal-to-noise ratio
SSCS	strict sense cyclo-stationary
s(t)	continuous parameter cyclo-stationary process
T	KP x KP carrier autocorrelation matrix
T _D	observation time
T _P	a positive real number called the period of a continuous parameter CS process
T _s	sampling interval
t _n	n'th sampling time
TR[·]	trace of the matrix in brackets
V	output of whitening filter
V'	output of weighting filter
W	whitening filter
WSCS	wide sense cyclo-stationary
x(t)	a real zero mean wide sense stationary Gauss-Markov process
Y	observation random process
y _n	elements of Y
Z[·]	log-likelihood ratio
$\tilde{Z}[\cdot]$	optimum decision variable (modified log-likelihood ratio)

LIST OF SYMBOLS (Cont.)

<u>Symbol</u>	<u>Definition</u>
Z_N	sum of the squares of N independent zero mean Gaussian random variables with different variances
$\tilde{Z}_S[\cdot]$	suboptimum decision variable
$\delta(t)$	Dirac delta function
β	starting time
Λ	real diagonal matrix of eigenvalues
$\phi[\cdot]$	optimum decision rule
$\Phi(\gamma)$	normal probability distribution function
	$\Phi(\gamma) = \frac{1}{\sqrt{2\pi}} \int_{-\infty}^{\gamma} e^{-t^2/2} dt$
$\Phi_{Z_N}(w)$	characteristic function of Z_N
$\Pi(\cdot)$	a monotonic function that maps infinity to infinity
$\Pi^{-1}(\cdot)$	inverse of $\Pi(\cdot)$
ρ_0	sample-to-sample correlation coefficient
ρ	period-to-period correlation coefficient, $\rho = \rho_S^P$
σ_0^2	variance of the decision variable under H_0
σ_1^2	variance of the decision variable under H_1
λ_n	eigenvalues
\sim	distributed according to
$*$	complex conjugate of the transpose

CHAPTER I

INTRODUCTION

1.1 Basic Problem

The fixed time forced choice detection of Gaussian random processes in additive Gaussian noise via the likelihood ratio reduces to interpreting a quadratic form when the signal and noise autocorrelation functions or matrices are known. The literature is full of different interpretations for this quadratic form (Refs. 1, 8, 16, 17, 19, 20, 21, 25, 26, 31).

The topic of this dissertation is the detector design for the fixed time forced choice detection of Gaussian Cyclo-Stationary (CS) processes in additive Gaussian noise. CS processes are those random processes possessing autocorrelation functions or matrices with a cyclic structure. A technique is presented that permits interpretation of the detector quadratic form in a manner that preserves the cyclic structure of the signal autocorrelation function or matrix.

1.2 Cyclo-Stationary Processes

The feature that distinguishes Cyclo-Stationary (CS) processes from other random processes is a cyclic structure in the autocorrelation function for continuous parameter CS processes and in the autocorrelation matrix for discrete parameter CS processes. This cyclic structure has a different manifestation for continuous and

discrete parameter CS processes.

1. 2. 1 Continuous Parameter Cyclo-Stationary Processes.

A complex nonstationary random process $\{s(t), t \in T_D\}$ is a Strict Sense Cyclo-Stationary (SSCS) process if and only if there exists a positive number, T_P , called the period such that the joint probability distribution of $\{s(t_1 + qT_P), s(t_2 + qT_P), \dots, s(t_n + qT_P)\}$ equals the joint probability distribution of $\{s(t_1), s(t_2), \dots, s(t_n)\}$ for any integer q so that the translated parameter values are also parameter values. A SSCS process appears to be a strict sense stationary process when observed at integral multiples of the period, T_P .

It is also possible to define a CS process with the concept of Wide-Sense Stationarity. A complex nonstationary random process $\{s(t), t \in T_P\}$ with autocorrelation function $R_s(t_1, t_2)$ is a Wide Sense Cyclo-Stationary (WSCS) process if and only if there exists a positive number, T_P , called the period such that $E\{|s(t)|^2\} < \infty$ for $t \in T_D$, $E\{s(t=qT_P)\} = E\{s(t)\}$, and $R_s(t_1 + qT_P, t_2 + qT_P) = R_s(t_1, t_2)$ for any integer q so that the translated parameter values are also parameter values. $E\{\}$ denotes the expected value of the quantity in brackets. A WSCS process appears to be a wide sense stationary process when observed at integral multiples of the period T_P .

The autocorrelation function of a WSCS process has a cyclic structure due to the wide sense stationary behavior of a WSCS process. The autocorrelation function of a SSCS process also has a cyclic

structure if $E\{|s(t)|^2\} < \infty$ for $t \in T_D$. It is the cyclic structure of the autocorrelation function of a CS (SSCS or WSCS) process that distinguishes a CS process from all other random processes. Contrast this to the autocorrelation function of a wide sense stationary periodic process, $R(\tau + T_P) = R(\tau)$. The second order statistics are equal when observed at time differences that are integral multiples of the period.

An example of a WSCS process is a clocked waveform (Ref. 24). Consider the clocked waveform $s(t)$ consisting of an elementary waveform $g(t)$ which is clocked at the rate T_P .

$$s(t) = \sum_{n=-\infty}^{\infty} a_n g(t - nT_P)$$

where $a_n = \pm 1$ with a probability of $1/2$.

$$E\{s(t)\} = \sum_{n=-\infty}^{\infty} E\{a_n\} g(t - nT_P) = 0 .$$

$$R_s(t_1, t_2) = E\{\tilde{s}(t_1)s(t_2)\} = \sum_{n, m=-\infty}^{\infty} R(m-n) g(t_1 - nT_P) g(t_2 - mT_P)$$

for $R(m-n) = E\{a_n a_m\}$.

$$R_s(t_1 + T_P, t_2 + T_P) = \sum_{n, m=-\infty}^{\infty} R(m-n) g[t_1 - (n-1)T_P] g[t_2 - (m-1)T_P] .$$

Let $n' = n-1$ and $m' = m-1$. Then

$$\begin{aligned}
R_s(t_1+T_P, t_2+T_P) &= \sum_{n', m'=-\infty}^{\infty} R(m'-n') g[t_1-n'T_P] g[t_2-m'T_P] \\
&= R_s(t_1, t_2) .
\end{aligned}$$

From this one can conclude that a clocked waveform consisting of clocked pulses, $g(t) = \delta(t)$, is a WSCS process, and any other clocked waveform can be generated by inputting clocked pulses into a filter with impulse response $g(t)$.

1.2.2 Discrete Parameter Cyclo-Stationary Processes. A

complex nonstationary random process $\{s(n); n=1, 2, 3, \dots, KP\}$ is a Strict Sense Cyclo-Stationary (SSCS) process if and only if there exists a nonzero integer, P , called the period such that the joint probability distribution of $\{s(1+qP), s(2+qP), \dots, s(n+qP)\}$ equals the joint probability distribution of $\{s(1), s(2), \dots, s(n)\}$ for any integer q so that the translated parameter values are parameter values.

It is again possible to define a CS process with the concept of Wide Sense Stationarity. A complex nonstationary random process $\{s(n); n=1, 2, 3, \dots, KP\}$ with autocorrelation matrix $R_S = \{r_s(n, m)\}$ for $n, m = 1, 2, 3, \dots, KP$ is a Wide Sense Cyclo-Stationary (WSCS) process if and only if there exists a nonzero integer, P , called the period such that $E\{|s(n)|^2\} < \infty$ for $n=1, 2, 3, \dots, KP$, $E\{s(n+qP)\} = E\{s(n)\}$, and $r_s(n+qP, m+qP) = r_s(n, m)$ for any integer q so that the translated parameter values are also parameter

values.

Just as in the continuous parameter case, a CS process appears to behave as a stationary (strict or wide sense stationarity) process when observed at integral multiples of the period P . The autocorrelation matrix of a WSCS process has a cyclic structure as does the autocorrelation matrix of a SSCS process if $E\{|s(n)|^2\} < \infty$. It is this cyclic structure that is a unique feature of CS processes.

1.2.3 Cyclic Structure of the Autocorrelation Matrix. CS

processes will refer to discrete parameter CS processes for the remainder of this dissertation unless indicated differently. The cyclic structure of the autocorrelation matrix of a CS process is expressible in a manner that permits factoring the autocorrelation matrix in a meaningful form.

Consider the CS process

$$\mathbf{S} = [s(1), s(2), \dots, s(P), \dots, s(KP)]^T$$

which is a column vector. \mathbf{S} has a period P and there are KP elements in the observation, i. e., there are K periods in the observation. The autocorrelation matrix is

$$R_{\mathbf{S}} = \{r_{\mathbf{S}}(u, v)\} \quad \text{for } u, v = 1, 2, 3, \dots, KP.$$

Subdivide $R_{\mathbf{S}}$ into $P \times P$ dimensional matrices A_{nm} for $n, m = 1, 2, 3, \dots, K$.

$$R_S = [A_{nm}] \quad \text{for } n, m = 1, 2, 3, \dots, K .$$

The A_{nm} have elements

$$A_{nm} = \left[r_s[(n-1)P+u, (m-1)P+v] \right] \quad \text{for } u, v = 1, 2, 3, \dots, P .$$

A_{nm} is the correlation matrix between the P elements in the n th period and the P elements in the m th period. The cyclic structure in R_S for CS processes is expressible as

$$\begin{aligned} A_{n+q, m+q} &= \left[r_s[(n+q-1)P+u, (m+q-1)P+v] \right] \\ &= \left[r_s[(n-1)P+u, (m-1)P+v] \right] \\ &= A_{nm} \end{aligned}$$

for q any integer such that $n+q$ and $m+q = 1, 2, 3, \dots, K$. It also follows that $A_{nn} = A$ for $n=1, 2, 3, \dots, K$. A is called the modulation autocorrelation matrix and is the autocorrelation matrix for any period. R_S then has the form

$$R_S = \begin{bmatrix} A & A_{12} & A_{13} & \dots & A_{1,K} \\ A_{12}^* & A & A_{12} & \dots & A_{1,K-1} \\ A_{13}^* & A_{12}^* & A & \dots & A_{1,K-2} \\ \vdots & \vdots & \vdots & \vdots & \vdots \\ A_{1,K}^* & A_{1,K-1}^* & A_{1,K-2}^* & \dots & A \end{bmatrix}$$

where $*$ denotes the complex conjugate of the transpose. This is the

cyclic structure that distinguishes CS processes (SSCS and WSCS) from all other random processes and permits factorizing R_S in a meaningful manner.

Since R_S is a positive definite Hermitian matrix, so is A a positive definite Hermitian matrix. There then exists a lower triangular matrix, M , called the modulation matrix such that

$$A = M^* M .$$

M is nonsingular because it is the square root of R_S . In order to show the key effect of M , all the A_{nm} can be written in terms of it. Let

$$T_{nm} = M^{*-1} A_{nm} M^{-1} ;$$

$$T_{nn} = I_P, \text{ the } P \times P \text{ identity matrix for} \\ n = 1, 2, 3, \dots, K$$

so that

$$A_{nm} = M^* T_{nm} M .$$

R_S is then factorable as

$$\begin{aligned}
R_S &= \begin{bmatrix} M^* & & & & \\ & M^* & & & \\ & & M^* & & \\ & & & \ddots & \\ & & & & M^* \end{bmatrix} \begin{bmatrix} I_p & T_{12} & T_{13} & \cdots & T_{1,K} \\ T_{12}^* & I_p & T_{12} & \cdots & T_{1,K-1} \\ T_{13}^* & T_{12}^* & I_p & \cdots & T_{1,K-2} \\ \vdots & \vdots & \vdots & \ddots & \vdots \\ T_{1,K}^* & T_{1,K-1}^* & T_{1,K-2}^* & \cdots & I_p \end{bmatrix} \begin{bmatrix} M & & & & \\ & M & & & \\ & & M & & \\ & & & \ddots & \\ & & & & M \end{bmatrix} \\
&= M_K^* T M_K.
\end{aligned}$$

M_K is a $KP \times KP$ dimensional matrix with the modulation matrix M repeated on the diagonal. T is $KP \times KP$ dimensional matrix of the T_{nm} 's. T is called the carrier autocorrelation matrix and indicates how to combine the information in the modulation autocorrelation matrix to form the A_{nm} 's. It also follows that T is a positive definite Hermitian matrix because R_S is positive definite Hermitian. There then exists a lower triangular matrix, C , called the carrier matrix such that

$$T = C^* C .$$

R_S is then factorable as

$$R_S = M_K^* C^* C M_K .$$

This is the form of the cyclic structure of the autocorrelation matrix of a CS process that is preserved in the detector design. An example of factoring the autocorrelation matrix of a CS process is presented

in Appendix E.

1.3 Generation of Cyclo-Stationary Processes

There are many ways of generating continuous and discrete parameter CS processes. It is the intent here to list a few of these ways.

1.3.1 Continuous Parameter Cyclo-Stationary Processes.

Four representative cases that produce CS processes are listed below:

1. Random processes describing propellor and reciprocating engine noise.
2. Amplitude-modulated random process, $s(t)$, of the form

$$s(t) = x(t) p(t) \quad \text{where}$$

$x(t)$ is a stationary random process, and $p(t)$ is a periodic function.

3. Random processes arising in meteorology.
4. Clocked waveforms described in Section 1.2.1.

1.3.2 Discrete Parameter CS Processes. Sampling continuous time random processes is the basic technique for generating discrete time CS processes in this dissertation. Discrete time CS process can arise either from sampling continuous time CS processes or from sampling continuous time stationary random processes in certain ways.

1.3.2.1 Sampling Continuous Parameter Cyclo-

Stationary Processes. Sampling continuous time CS processes must be performed in a prescribed manner if the cyclic structure exhibited by CS process is to be preserved. The CS process must be sampled so that there are exactly an integral number of samples, P , in each period of the process. Let T_s and T_P be the sampling interval and the period of the sampled continuous time CS process respectively. Then $PT_s = T_P$ if the cyclic structure is to be preserved. The time that the sampling started must also be known in order to calculate the autocorrelation matrix.

1.3.2.2 Sampling Continuous Stationary Random Processes.

Multiplexing samples from each of the sensors of a P sensor array which is observing a stationary random process generates a CS process with a period P . The modulation correlation matrix A is the autocorrelation of the samples taken at the same sampling instant from each of the P sensors. The form of A arises from the spatial modulation introduced by the location of the observed stationary random process with respect to the sensors. A_{nm} is the correlation matrix of the samples taken from the P sensors at the n th and m th sampling instants. The form of A_{nm} also arises from the spatial modulation introduced by the array geometry when the stationary random process is observed at the n th and m th sampling instants.

The array processing problem is well understood and extensively studied (Refs. 3, 6, 21, 28, 29, 30). Studying the array

processing problem as a problem in detecting CS processes is expected to only add new insight and not new knowledge.

It is also possible to generate a CS process with period P by multiplexing samples from P different stationary random processes. The A matrix is the autocorrelation matrix of the P samples taken at a sampling instant, and A_{nm} is the correlation matrix between the P samples taken at the n th and m th sampling instants.

1.4 Procedure

The criteria for receiver design and accepting observations is presented to prevent confusion in future discussions. The optimum detector presented in this dissertation is designed according to the likelihood ratio. There are many criteria such as the Bayes, Neyman-Pearson, and Weighted Combination to name a few that support the likelihood ratio as the optimum decision rule for a detector. Birdsall (Ref. 2) showed that the detector which bases its decisions on the likelihood ratio yields optimum performance for the class of criteria which considers correct decisions "good" and incorrect decisions "bad." The three criteria listed above fall into this class of criteria.

The observations used in designing and operating the receiver are finite length vectors. There is no interest in this dissertation in considering any continuous time forms of the detector. The vectors are transformations, such as sampling, of the continuous time random

processes actually observed. The transformations must preserve the Cyclo-Stationary properties of the continuous time random processes.

1.5 Historical Background

The literature on detecting Cyclo-Stationary processes is sparse. Surprisingly little of that deals with optimum detectors.

Deutch (Ref. 9) studies the demodulation of CS processes resulting from the amplitude modulation of a stationary random process by a periodic function. It is shown that a linear filter may be used to enhance a CS process out of several interfering CS processes.

Parzen and Shirer (Ref. 22) generalize Deutch's work by covering the frequency band occupied by the CS process in question with several filters non-overlapping in frequency followed by square law detectors.

Kincaid (Ref. 18) derives the optimum detector for a specific CS process in additive Gaussian noise. The periods of the CS process are statistically related in the first order Markov sense. The detector is specialized for the small signal-to-noise ratio case and a suboptimum approximation to this is evaluated. The suboptimum detector is a circulating delay line preceded by a signal enhancer and noise processor and is followed by an energy detector.

Hariharan (Ref. 13) states that all detectors are basically

nonlinear devices. He concentrates on studying the output signal-to-noise ratio at the output of a v th law device for Gaussian CS processes and additive Gaussian noise at the input.

The dissertation by Hurd (Ref. 14) is an excellent study on the mathematical properties of CS processes. There is also an extensive analysis of spectral analysis and estimation of CS processes.

1.6 Organization of This Study

Background material is presented in Chapter II. This includes a quick review of detection theory and a presentation of some important evaluation techniques. The optimum detector is designed and discussed in Chapter III. In Chapter IV, a signal-and-noise model are presented and used to evaluate the optimum detector performance. A suboptimum detector is presented and evaluated in Chapter V. Chapter VI contains the summary and conclusions, contributions of this study, and suggestions for future work.

1.7 Notation

The basic notation for the remainder of the dissertation is defined. All vectors are column vectors unless otherwise noted and are written as the transpose of a row vector. All vectors and matrices are denoted by capital letters. The exact meaning will be clear by the context. Given a matrix U , U^T is the transpose; \bar{U} is the complex conjugate; U^* is the complex conjugate of U^T ; and

$|U|$ is the determinant.

All observations are complex valued random vectors with KP elements. The signal and noise vectors are S and N respectively with elements

$$S = \{s_1, s_2, \dots, s_{KP}\}^T, \quad \text{and}$$

$$N = \{n_1, n_2, \dots, n_{KP}\}^T \quad \text{where}$$

s_q and n_q are complex valued single observations. The signal and noise correlation matrices are R_S and R_N respectively. R_S and R_N are Hermitian positive definite matrices.

$$R_S = E [S - E\{S\}] [S - E\{S\}]^*$$

and

$$R_N = E [N - E\{N\}] [N - E\{N\}]^*$$

where $E\{ \}$ denotes expectation.

The symbol \sim denotes "is distributed according to." An example is the normal probability distribution function.

$$X \sim N(M, R)$$

indicates that the vector X is distributed according to the multivariate normal probability distribution function with mean vector M and correlation matrix R .

CHAPTER II
BACKGROUND

2.1 Review of Detection Theory

The pertinent facts of signal detection theory are reviewed in order to present the techniques used in this dissertation. Classical fixed-time forced-choice signal detection theory was aptly formulated by Peterson, Birdsall, and Fox (Ref. 23) in 1954. The theory has since been extensively refined and extended. The basic signal detection situation is presented schematically in Fig. 2.1.

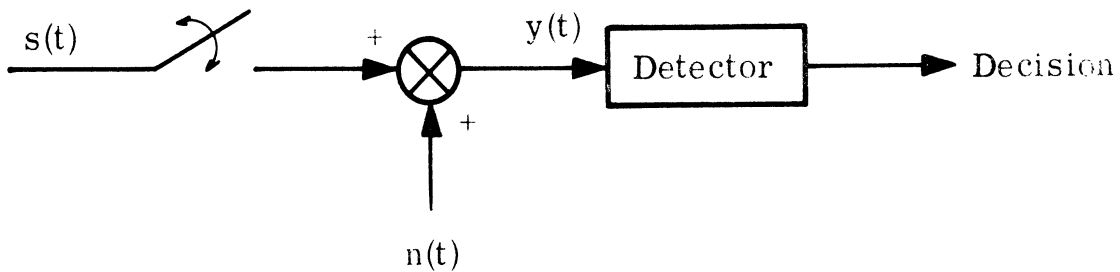


Fig. 2.1. Illustration of the basic signal detection problem

The noise process is $n(t)$, and $s(t)$ is the signal process. The detector is presented with an observation $y(t)$ during the time interval β and $\beta + T_D$. The observation either consists of noise alone, hypothesis H_0 , or signal and noise, hypothesis H_1 . When the signal is present, it is present for the entire observation interval. The hypotheses are mutually exclusive. At the end of the observation

interval, the detector must decide whether the signal is present or absent, that is which of the two possible hypotheses is in effect. The signal detection problem can be expressed as a hypothesis testing problem which is expressible in shorthand as:

$$y(t) = \begin{cases} n(t) & , \quad H_0 \\ s(t) + n(t) & , \quad H_1 \end{cases} \quad \beta \leq t \leq \beta + T_D .$$

The random process $y(t)$ is customarily described by a vector representation in order to use statistical decision theory. According to the Shannon sampling theorem, $y(t)$ can be represented as the vector

$$Y = \{y_1, y_2, y_3, \dots, y_N\}^T ,$$

where

$$N = 2WT$$

and

$$y_n = y \left(\beta + \frac{1-n}{2W} \right) \quad \text{for } n = 1, 2, 3, \dots, N ,$$

if $y(t)$ is timelimited to an interval of length T and Fourier Series bandlimited to an interval of width W .

2.1.1 Detector Design. Birdsall (Ref. 2) showed that the detector which bases its decisions on the likelihood ratio yields

optimum performance for the class of criteria which considers correct decisions "good" and incorrect decisions "bad." Three commonly used criteria that fall into this category are the Bayes, Neyman-Pearson, and Weighted Combination criteria. The optimum decision rule is

$$\phi[Y] = \begin{cases} 1, & L[Y] > c \\ r, & L[Y] = c \\ 0, & L[Y] < c \end{cases}$$

where

1. $L[Y] = \frac{f[Y | H_1]}{f[Y | H_0]}$ is the likelihood ratio.
2. $f[Y | H_i]$ is the observation probability density function under hypothesis H_i for $i = 0$ and 1 .
3. c is the pre-assigned threshold.
4. $\phi[Y]$ is the probability of deciding that a signal is present given the observation Y .
5. $0 \leq r \leq 1$.

The case for $L[Y] = c$ describes a randomized decision rule.

The threshold c is selected according to the chosen criteria.

Birdsall (Ref. 2) has also shown that the detector which bases its decisions on a monotonic function of the likelihood ratio also yields optimum performance. The monotonic function must map infinity to

infinity. This property is referred to as the monotone property of likelihood ratios in this dissertation.

2.1.2. Detector Evaluation. Detector performance is succinctly summarized by the receiver operating characteristic (ROC). The ROC is a plot of the probability of false alarm, P_{FA} , versus the probability of detection, P_D . P_{FA} is the probability of deciding hypothesis H_1 occurred when hypothesis H_0 occurred, and P_D is the probability of deciding H_1 occurred when indeed it did. Birdsall (Ref. 2) showed that the ROC of all likelihood ratio detectors is convex.

For any detector,

$$P_D = E \{ \phi[Y] | H_1 \} \quad (2.1)$$

and

$$P_{FA} = E \{ \phi[Y] | H_0 \} \quad (2.2)$$

where $\phi[Y]$ is the decision rule. P_D and P_{FA} become

$$P_D = \int_{L[Y] \geq c}^{\infty} f[Y | H_1] d Y \quad (2.3)$$

and

$$P_{FA} = \int_{L[Y] > c}^{\infty} f[Y | H_0] d Y \quad (2.4)$$

for a likelihood ratio detector if and only if the probability that $L[Y] = c$ is zero. Let $\Pi(\cdot)$ be a monotonic function that maps infinity to infinity and

$$\Pi'[Y] = \Pi[L[Y]] \quad . \quad (2.5)$$

Equations 2.3 and 2.4 then become

$$P_D = \int_{c'}^{\infty} f[\Pi'|H_1] d\Pi' \quad (2.6)$$

and

$$P_{FA} = \int_{c'}^{\infty} f[\Pi'|H_0] d\Pi' \quad (2.7)$$

where $c' = \Pi(c)$. These relations can be further simplified by a theorem proved by Birdsall (Ref. 2) which states that the likelihood ratio of a monotonic function of the likelihood ratio is the likelihood ratio. That is

$$L[Y] = \frac{f\left\{\Pi[L[Y]] \mid H_1\right\}}{f\left\{\Pi[L[Y]] \mid H_0\right\}} \quad . \quad (2.8)$$

Substitute Eqs. 2.5 and 2.8 into Eqs. 2.6 and 2.7.

$$P_D = \int_{c'}^{\infty} \Pi^{-1}[\Pi'] f[\Pi'|H_0] d\Pi' \quad (2.9)$$

and

$$P_{\text{FA}} = \int_{c'}^{\infty} f[\Pi' | H_0] d\Pi' \quad (2.10)$$

where $\Pi^{-1}(\cdot)$ is the inverse of the function $\Pi(\cdot)$. It is then seen that the ROC for the optimum detector is completely specified once $f[\Pi' | H_0]$ is known.

2.1.3 Normal ROC. The normal ROC is a standard for comparing ROC's because it is parameterized by one parameter, d' . A ROC is called normal if it can be parameterized by the normal distribution as:

$$P_{\text{D}} = \Phi(\lambda + d')$$

and

$$P_{\text{FA}} = \Phi(\lambda)$$

where

$$\Phi(\lambda) = \frac{1}{\sqrt{2\pi}} \int_{-\infty}^{\lambda} e^{-x^2/2} dx .$$

The parameter d' is called the detectability index though sometime it is referred to as the quality of detection. Normal ROC's are usually plotted on normal-normal graph paper because normal ROC's plot as straight lines. A family of normal ROC's with detectability index d' is plotted in Fig. 2.2.

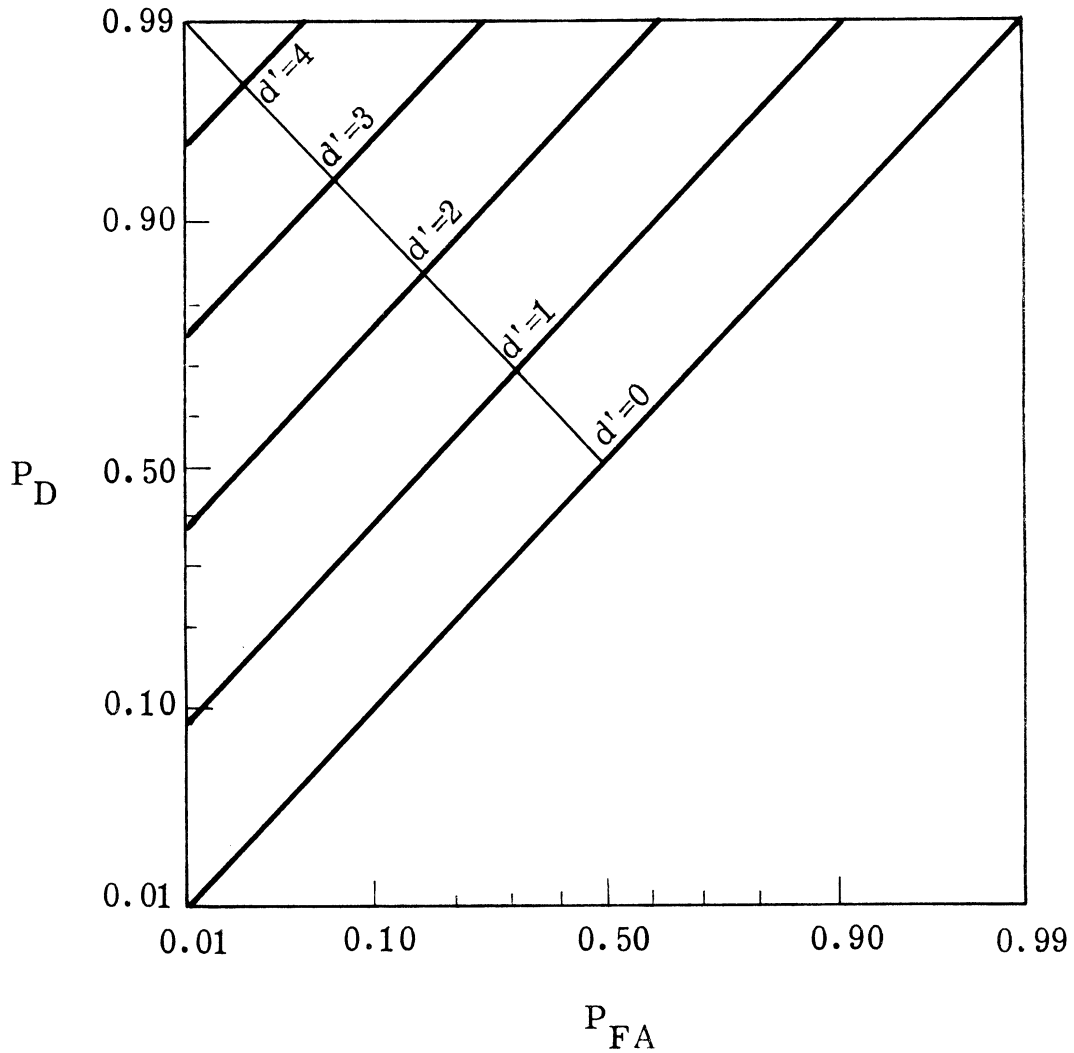


Fig. 2.2. Normal ROC's with detectability index d'

Physical significance can be attributed to d' , and this accounts for the attractiveness of normal ROC's. The performance of the optimum detector for signal known exactly in white Gaussian noise is described by a normal ROC with

$$d' = \sqrt{\frac{2E}{N_0}}$$

where E is the signal energy and N_0 is the noise power per hertz.

The normal ROC provides a convenient quantitative measure of performance for the comparison of ROC's. When ROC's are almost normal, an equivalent detectability index, d'_e , as measured on the negative diagonal, $P_D + P_{FA} = 1$, indicates the performance.

2.1.4 Binormal ROC. The binormal ROC appears in many situations as the result of normal ROC's and the use of normal-normal graph paper for plotting ROC's. On normal-normal graph paper, normal ROC curves plot as a straight line with a slope of unity while binormal ROC curves plot as a straight line with a slope less than unity. Consequently binormal ROC's can be parameterized by a SLOPE and a detectability index $d'_e \cdot d'_e$ is that point where the binormal ROC curve intersects the negative diagonal, $P_D + P_{FA} = 1$. A few binormal ROC's are presented in Fig. 2.3.

The binormal ROC arises in situations where the decision variable is normal under H_0 and H_1 but with different first and second order moments under H_0 and H_1 . Let Z be the decision variable. A binormal ROC arises when

$$Z \sim \begin{cases} N(m_0, \sigma_0^2), & H_0 \\ N(m_1, \sigma_1^2), & H_1 \end{cases} .$$

d'_e and SLOPE are (see Appendix C)

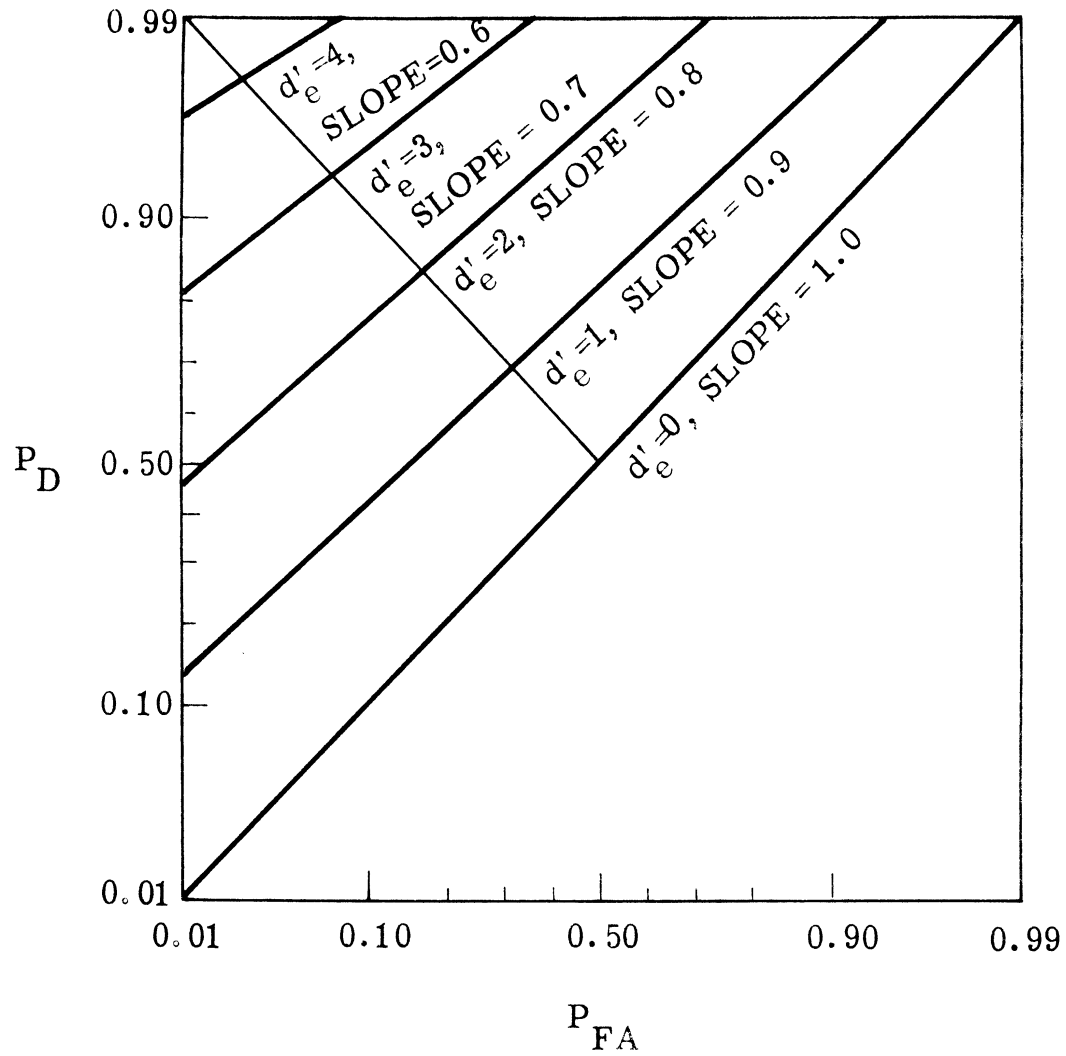


Fig. 2.3. Binormal ROC's with detectability index d'_e and slope SLOPE

$$d'_e = \frac{2(m_1 - m_0)}{\sigma_1 + \sigma_0} \quad (2.11)$$

and

$$\text{SLOPE} = \sigma_0 / \sigma_1 \quad (2.12)$$

SLOPE is a measure of the difference in the variance of, and d'_e is a measure of the difference in the mean of Z under H_0 and H_1 .

The binormal ROC is not convex and consequently cannot be the ROC of likelihood ratio detector (Ref. 2). However a region of the optimum ROC may behave as a binormal ROC. It then becomes convenient to label and to parameterize the optimum ROC by a d'_e and a SLOPE in this region.

2.2 Performance Evaluation and Characteristic Functions

The statistics of the decision variable, Z , under H_0 and H_1 must be known to generate the ROC. Many times Z , under H_0 and H_1 , is the sum of the squares of independent zero mean Gaussian random variables with different variances. The probability density function of the sum of the squares of independent zero mean Gaussian random variables with different variances is a noncentral chi-square distribution. The noncentral chi-square probability density function is well known in the form of series expansions (Ref. 15). Use of the series expansions for the probability density functions require approximations in the form of truncating the series. A different technique is presented for approximating this probability density function numerically. The ROC may then be generated by Eqs. 2.9 and 2.10 or Eqs. 2.1 and 2.2 depending if Z is or is not respectively the optimum decision variable.

Let

$$Z_N = \sum_{n=1}^N x_n^2$$

where

1. The x_n are independent.
2. $x_n \sim N(0, \sigma_n^2)$.

Let $f[Z_N]$ be the probability density function of Z_N ; $\Phi_{Z_N}(w)$ the characteristic function of Z_N ; and $\Phi_{x_n}(w)$ the characteristic function of x_n . The characteristic function of Z_N is defined as

$$\Phi_{Z_N}(w) = \int_{-\infty}^{\infty} f(Z_N) e^{jwZ_N} dZ_N . \quad (2.13)$$

It then follows that

$$f(Z_N) = \frac{1}{2\pi} \int_{-\infty}^{\infty} \Phi_{Z_N}(w) e^{-jwZ_N} dw . \quad (2.14)$$

Since x_n are independent,

$$\Phi_{Z_N}(w) = \prod_{n=1}^N \Phi_{x_n}(w) . \quad (2.15)$$

The x_n^2 are chi-square random variables with characteristic function (Ref. 7)

$$\Phi_{x_n}(w) = \frac{1}{\sqrt{1 - j2\sigma_n^2 w}} \quad (2.16)$$

Substitute Eq. 2.16 into Eq. 2.15.

$$\Phi_{Z_N}(w) = \prod_{n=1}^N \frac{1}{\sqrt{1 - j2\sigma_n^2 w}} \quad (2.17)$$

$f[Z_N]$ follows by substituting Eq. 2.17 into Eq. 2.14.

$f[Z_N]$ is evaluated numerically from Eqs. 2.17 and 2.14.

Equation 2.14 is evaluated by using the Fast Fourier Transform algorithm at a considerable saving in computer time over using the Discrete Fourier Transform (Refs. 4 and 5).

CHAPTER III
THE OPTIMUM DETECTOR FOR WIDE SENSE
CYCLO-STATIONARY PROCESSES

3.1 Introduction

The optimum detector for Gaussian WSCS processes in additive Gaussian noise is derived using the likelihood ratio as the optimum decision rule. The detector is derived in a manner that isolates the cyclic structure of the signal correlation matrix. The detector for WSCS processes has the form of noise reduction followed by signal enhancement followed by energy detection.

3.2 Detector Design

The detector problem is a fixed time forced choice detection problem with completely known statistics. Observations are gathered until there are KP observations at which time a decision must be made as to the absence or presence of a signal. The detector design is based on the optimum decision rule, the likelihood ratio. The signal is a zero mean complex Gaussian WSCS process, S , with autocorrelation matrix R_S . The noise, N , is also a zero mean complex Gaussian process with autocorrelation matrix R_N and is independent of the signal. The observation, Y , under the hypotheses H_0 and H_1 is

$$Y = \begin{cases} N & , H_0 \\ S + N & , H_1 \end{cases} .$$

The observation statistics under H_0 and H_1 are

$$Y \sim \begin{cases} N[0, R_N] & , H_0 \\ N[0, R_S + R_N] & , H_1 \end{cases} .$$

The detector is designed in two steps. The first step is deriving the sufficient statistic for making optimum decisions and presenting three common interpretations of the sufficient statistic. The second step is expanding the sufficient statistic in a manner that permits preserving the cyclic structure of R_S in the detector.

3.2.1 The Sufficient Statistic and Three Common Interpretations. The observation statistics are required to form the likelihood ratio, $L[Y]$. The observation statistics are:

$$f[Y|H_0] = (2\pi)^{-KP/2} |R_N|^{-\frac{1}{2}} \exp\{-Y^* R_N^{-1} Y/2\} ,$$

and

$$f[Y|H_1] = (2\pi)^{-KP/2} |R_S + R_N|^{-\frac{1}{2}} \exp\{-Y^* [R_S + R_N]^{-1} Y/2\} .$$

The likelihood ratio is defined as

$$L[Y] = f[Y|H_1] / f[Y|H_0] ,$$

and

$$L[Y] = \left[|R_N| / |R_S + R_N| \right]^{\frac{1}{2}} \exp \left\{ Y^* \left[R_N^{-1} - [R_S + R_N]^{-1} \right] Y/2 \right\}.$$

The log-likelihood ratio, Z , is defined as

$$Z[Y] = \ln \left[L[Y] \right].$$

By the monotone property of likelihood ratios discussed in Section 2.2.1, Z is a sufficient statistic for making optimum decisions.

$$Z[Y] = 1/2 \ln \left[|R_N| / |R_S + R_N| \right] + Y^* \left[R_N^{-1} - [R_S + R_N]^{-1} \right] Y/2.$$

Since all the matrices, R_S and R_N , are known, $1/2 \ln \left[|R_N| / |R_S + R_N| \right]$ is a known constant. Consequently by the monotone property of likelihood ratios, a sufficient statistic for making optimum decisions is the modified log-likelihood ratio, $\tilde{Z}[Y]$, where

$$\tilde{Z}[Y] = Y^* \left[R_N^{-1} - [R_S + R_N]^{-1} \right] Y. \quad (3.1)$$

The sufficient statistic, $\tilde{Z}[Y]$, is a quadratic form. $\tilde{Z}[Y]$ must be interpreted in a manner to isolate R_S and preserve the cyclic structure of R_S . Three frequently mentioned interpretations of $\tilde{Z}[Y]$ are presented below as a contrast to the interpretations presented

in this dissertation.

1. Triangularization

If $R_N^{-1} - [R_S + R_N]^{-1}$ is a positive Hermitian matrix, there exists (Ref. 11) a lower triangular matrix, B , such that

$$R_N^{-1} - [R_S + R_N]^{-1} = B^* B .$$

The detector becomes an energy detector with filtering,

$$\tilde{Z}[Y] = \|B Y\|^2 ,$$

and is shown in Fig. 3.1.

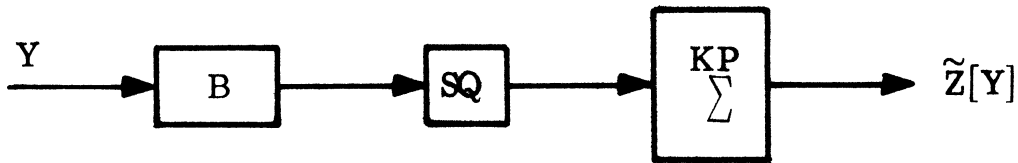


Fig. 3.1. Triangularization

2. Simultaneous Diagonalization

Let R_N^{-1} be a positive definite Hermitian matrix and $[R_S + R_N]^{-1}$ be a Hermitian matrix. There then exists (Appendix A) a matrix D and a real diagonal matrix, Ψ , such that

$$R_N^{-1} = D^* D ,$$

and

$$[R_S + R_N]^{-1} = D^* \Psi D .$$

$\tilde{Z}[Y]$ becomes

$$\tilde{Z}[Y] = \left\| [I - \Psi]^{-\frac{1}{2}} DY \right\|^2 .$$

$\tilde{Z}[Y]$ is still an energy detector with prefiltering. In this interpretation, there is a term identifiable with the input signal-to-noise ratio.

The detector is implemented in Fig. 3.2.

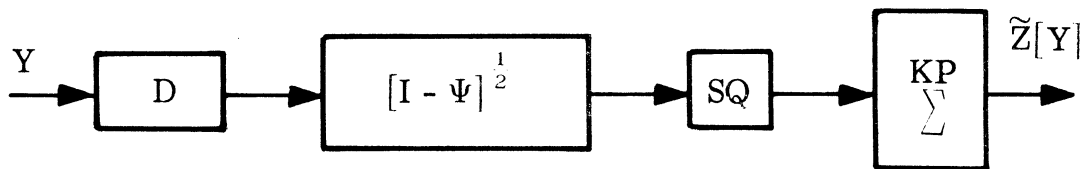


Fig. 3.2. Simultaneous diagonalization

3. Estimator-Correlator

Given

$$Y = S + N ,$$

Kailath (Ref. 16) shows that the linear filter, H , that generates the minimum mean-square estimate, \hat{S} , of S from Y has the form

$$\begin{aligned} H &= R_S [R_S + R_N]^{-1} \\ &= I - R_N [R_S + R_N]^{-1} . \end{aligned} \quad (3.2)$$

Multiply both sides of Eq. 3.2 on the left by R_N^{-1} and rearrange.

$$R_N^{-1} H = R_N^{-1} - [R_S + R_N]^{-1} \quad (3.3)$$

Substitute Eq. 3.3 into Eq. 3.1.

$$\tilde{Z}[Y] = Y^* R_N^{-1} H Y \quad (3.4)$$

If R_N^{-1} is a positive definite Hermitian matrix, it can be triangularized (Ref. 12).

$$R_N^{-1} = F^* F$$

where F is lower triangular. Consequently Eq. 3.4 becomes

$$\tilde{Z}[Y] = [Y^* F^*] [F \hat{S}]$$

where $\hat{S} = H Y$. Besides providing a sufficient statistic for making optimum decisions, this interpretation for $\tilde{Z}[Y]$ also generates the minimum mean-square estimate of S . The block diagram for $\tilde{Z}[Y]$ is shown in Fig. 3.3.

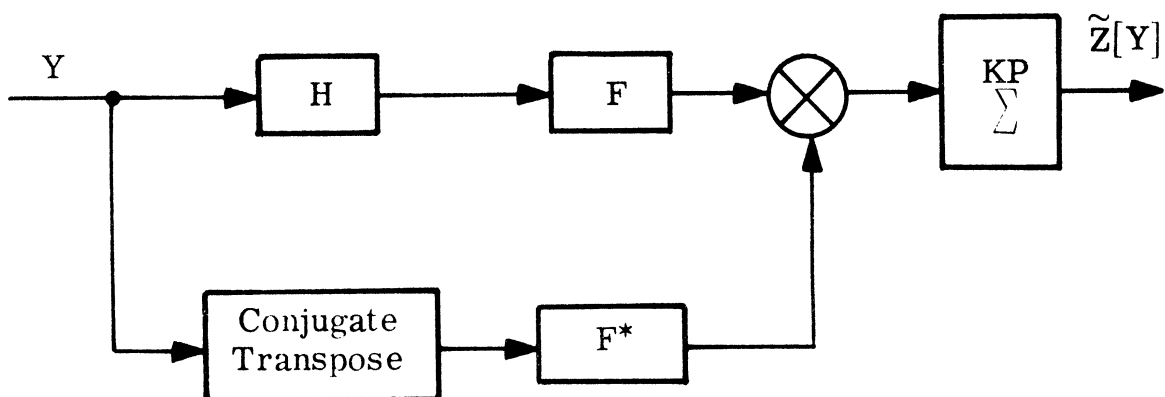


Fig. 3.3. Estimator-correlator

3. 2. 2 Expansion of the Sufficient Statistic. To preserve the cyclic structure of R_S , $\tilde{Z}[Y]$ must be expanded to isolate R_S . The expression for $\tilde{Z}[Y]$ is repeated below.

$$\tilde{Z}[Y] = Y^* \left[R_N^{-1} - [R_S + R_N]^{-1} \right] Y \quad (3.1)$$

R_S must be isolated in $R_N^{-1} - [R_S + R_N]^{-1}$ in order to isolate R_S in $\tilde{Z}[Y]$. This can be partially accomplished by use of the following matrix identity. R_S and R_N are both positive definite. Then

$$[R_S + R_N]^{-1} = R_N^{-1} - R_N^{-1} [R_S^{-1} + R_N^{-1}]^{-1} R_N^{-1} \quad (3.3)$$

Substitute Eq. 3.3 into Eq. 3.1. $\tilde{Z}[Y]$ becomes

$$\tilde{Z}[Y] = Y^* R_N^{-1} [R_S^{-1} + R_N^{-1}]^{-1} R_N^{-1} Y \quad (3.4)$$

Now R_S must be further isolated in order to preserve the cyclic structure of R_S .

R_S is a positive definite Hermitian matrix and R_N is a positive definite. There then exists a matrix of eigenvectors, Q , and a real diagonal matrix of eigenvalues, Λ , such that (Appendix A)

$$R_S = Q^* Q \quad ,$$

and

$$(3.5)$$

$$R_N = Q^* \Lambda Q$$

Since R_S is the correlation matrix of a WSCS process, it can also be expressed as

$$R_S = M_K^* C^* C M_K$$

where M_K and C are lower triangular matrices. It is then possible to find (Appendix A) a unitary matrix, W , such that

$$Q = W C M_K \quad (3.6)$$

Substitute Eq. 3.6 into Eqs. 3.5 and then substitute into $[R_S^{-1} + R_N^{-1}]^{-1}$ of Eq. 3.4. $\tilde{Z}[Y]$ then becomes

$$\begin{aligned} \tilde{Z}[Y] &= Y^* R_N^{-1} M_K^* C^* W^* [I + \Lambda^{-1}]^{-1} W C M_K R_N^{-1} Y \\ &= \left\| [I + \Lambda^{-1}]^{-\frac{1}{2}} W C M_K R_N^{-1} Y \right\|^2. \end{aligned} \quad (3.7)$$

The cyclic structure of R_S is thus isolated in the terms $C M_K$.

The detector is implemented as shown in Fig. 3.4.

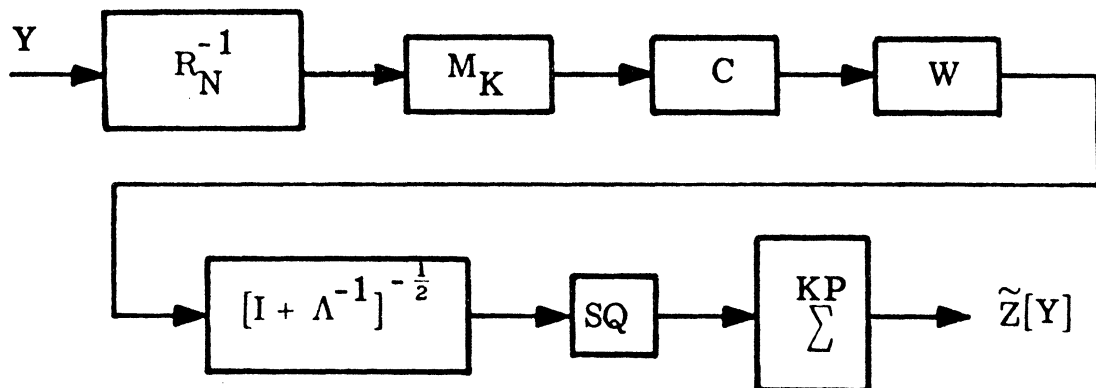


Fig. 3.4. Optimum detector for WSCS processes

3.3 Detector Description

The optimum detector for WSCS processes designed in Section 3.2 is described. Each of the detector blocks appearing in Fig. 3.4 is called a filter and is explained separately.

Noise Reduction

R_N^{-1} is a noise reduction filter. The noise reduction has the character of reducing the input power spectrum to R_N^{-1} by the square of the noise power spectrum. If the noise power spectrum is stable with a few large isolated spikes, the noise reduction takes on the character of a notch filter. It should be noted that this filter is unrealizable in the sense that future inputs are required to form the present output.

Signal Enhancement

The filter combination $M_K C$ is a signal enhancement filter. The signal enhancement has the character of enhancing the input power spectrum to $M_K C$ by the signal power spectrum. For WSCS processes the structure of the signal enhancement is identifiable with the cyclic structure of R_S .

M_K is a modulation emphasis filter. It emphasizes each period (P elements) of its input by the modulation matrix M .

C is a combining filter. It combines periods of its input, which have each been emphasized by M , according to the carrier matrix.

Whitening

W is a whitening filter. It whitens in the sense that under either H_0 or H_1 , the output vector has independent components with different variances. Let

$$V = W C M_K R_N^{-1} Y \quad (3.8)$$

with autocorrelation matrix R_V .

$$\begin{aligned} R_V &= E\{V V^*\} \\ &= W C M_K R_N^{-1} E\{Y Y^*\} R_N^{-1} M_K^* C^* W^* \end{aligned} \quad (3.9)$$

$$E\{Y Y^*\} = \begin{cases} M_K^* C^* \Lambda C M_K & , H_0 \\ M_K^* C^* [I + \Lambda] C M_K & , H_1 \end{cases} \quad (3.10)$$

Substitute Eqs. 3.10 into Eq. 3.9. Then

$$R_V = \begin{cases} \Lambda^{-1} & , H_0 \\ \Lambda^{-1} [I + \Lambda]^{-1} & , H_1 \end{cases} \quad (3.11)$$

and the elements of V are independent for the Gaussian input Y under H_0 and H_1 .

It should again be noted that W is an unrealizable filter.

Weighting

$[\mathbf{I} + \mathbf{\Lambda}^{-1}]^{-\frac{1}{2}}$ is a weighting filter. $\mathbf{\Lambda}$ is a real diagonal matrix with diagonal elements, λ_n , the noise-to-signal ratio behavior on the n th eigenvector. The eigenvector noise-to-signal ratio is inversely proportional to the input signal-to-noise ratio (Appendix D). If the input signal-to-noise ratio is small, the λ_n are large, and

$$[\mathbf{I} + \mathbf{\Lambda}^{-1}]^{-\frac{1}{2}} \approx \mathbf{I} \quad (3.12)$$

where \approx is read "approximately equal to." On the other hand if the input signal-to-noise ratio is large, λ_n are small, and

$$[\mathbf{I} + \mathbf{\Lambda}^{-1}]^{-\frac{1}{2}} \approx \mathbf{\Lambda}^{\frac{1}{2}} . \quad (3.13)$$

The weighting filter modifies the detector structure for departure from from the small input signal-to-noise ratio case.

The detector structure in Fig. 3.4 with the weighting filter bypassed is the small input signal-to-noise ratio approximation of the detector. This is an attractive feature in the sense that the small input signal-to-noise ratio form of the detector is directly identifiable without making approximations to all the filters.

3.4 Summary

The optimum detector for Gaussian WSCS processes in additive Gaussian noise is designed so as to preserve the cyclic structure of the signal autocorrelation matrix. The detector is a noise

reduction filter followed by a signal enhancement filter followed by an energy detector. The structure of the signal enhancement filter is clearly identifiable with the cyclic structure of the signal autocorrelation matrix. The low input signal-to-noise ratio form of the detector is directly identifiable by making an approximation in only one of the detector filters.

CHAPTER IV

PERFORMANCE EVALUATION OF THE OPTIMUM DETECTOR

4.1 Introduction

The performance of the optimum detector is evaluated and explained. A signal model is described for use in evaluating the performance, and expressions for characterizing performance are derived.

4.2 Model Description

The signal and noise models are selected to permit meaningful detector evaluation with a minimum number of parameters.

4.2.1 Noise Model. The noise model is selected to permit identification of performance characteristics with the signal model characteristics. The noise model selected is a real zero mean wide sense stationary white Gaussian noise with power spectral density N_0 .

4.2.2 Signal Model. The signal model selected is a real zero mean WSCS Gauss-Markov process. This model is selected because the behavior of the correlation function is completely characterized by the correlation coefficient.

The signal, S , is the sampled version of the time continuous WSCS process

$$s(t) = x(t) \cos (2\pi f_0 t + \beta) .$$

$x(t)$ is a real zero mean wide-sense stationary Gauss-Markov process with autocorrelation function $R_x(\tau) = R_x(0) e^{-\alpha|\tau|}$, and β and f_0 are known. The autocorrelation function of $s(t)$ is

$$R_s(t_n, t_m) = \frac{R_x(t_m - t_n)}{2} \left[\cos[2\pi f_0(t_m + t_n) + 2\beta] + \cos 2\pi f_0(t_m - t_n) \right].$$

Sample $s(t)$ at the rate $T_s = \frac{1}{Pf_0}$ so that there are P samples in a period $1/f_0$. Sample at the time instants $t_n = T_s(n-1)$ until there are KP samples, i.e., $n = 1, 2, 3, \dots, KP$. The autocorrelation matrix of S is R_S with elements $r_s(\theta, \phi)$ for $\theta, \phi = 1, 2, 3, \dots, KP$.

$$r_s(\theta, \phi) = \frac{R_x(0)}{2} \rho_s^{|\phi - \theta|} \left[\cos \left[\frac{2\pi}{P} (\phi + \theta - 2) + 2\beta \right] + \cos \frac{2\pi}{P} (\phi - \theta) \right]$$

where $\rho_s = R_x(1/Pf_0)/R_x(0)$ is the sample-to-sample correlation coefficient. $\rho_s^n = R_x(n/Pf_0)/R_x(0)$. Subdivide R_S into $P \times P$ submatrices A_{nm} for $n, m = 1, 2, 3, \dots, K$.

$$A_{nm} = \left[r_s[(n-1)P+u, (m-1)P+v] \right], \quad u, v = 1, 2, 3, \dots, P.$$

Now

$$\begin{aligned}
 r_s[(n-1)P+u, (m-1)P+v] &= \\
 \frac{R_x(0)}{2} \rho_s^{|(m-n)P+v-u|} &\left\{ \cos\left[\frac{2\pi}{P} [(m+n-2)P+u+v] + 2\beta\right] + \cos\frac{2\pi}{P} \right. \\
 &\left. [(m-n)P+v-u] \right\} \\
 = \frac{R_x(0)}{2} \rho_s^{|(m-n)P+v-u|} &\left\{ \cos\left[\frac{2\pi}{P} (u+v) + 2\beta\right] + \cos\frac{2\pi}{P} (v-u) \right\} .
 \end{aligned}$$

Consider the following three cases for $r_s[(n-1)P+u, (m-1)P+v]$.

1. $n = m$

$$\begin{aligned}
 r_s[(n-1)P+u, (n-1)P+v] &= \frac{R_x(0)}{2} \rho_s^{|v-u|} \left\{ \cos\left[\frac{2\pi}{P} (u+v) + 2\beta\right] \right. \\
 &\left. + \cos\frac{2\pi}{P} (v-u) \right\}
 \end{aligned}$$

2. $n = 1, m = 2$

$$r_s[u, P+v] = \frac{R_x(0)}{2} \rho_s^{|P+v-u|} \left\{ \cos\frac{2\pi}{P} [(u+v) + 2\beta] + \cos\frac{2\pi}{P} (v-u) \right\}$$

3. $m > n$

$$\begin{aligned}
r_s[(n-1)P+u, (m-1)P+v] &= \frac{R_x(0)}{2} \rho_s^{|(m-n)P+v-u|} \left\{ \cos \left[\frac{2\pi}{P} (u+v) + 2\beta \right] \right. \\
&\quad \left. + \cos \frac{2\pi}{P} (v-u) \right\} \\
&= \rho^{|m-n-1|} \frac{R_x(0)}{2} \rho_s^{|P+v-u|} \\
&\quad \left\{ \cos \left[\frac{2\pi}{P} (u+v) + 2\beta \right] + \cos \frac{2\pi}{P} (v-u) \right\}
\end{aligned}$$

where

$\rho = \rho_s^P$ is the period-to-period correlation coefficient.

It is possible to conclude from these three cases that for a WSCS Gauss-Markov process

$$A_{nm} = \begin{cases} \rho^{|m-n-1|} A_{12} & m > n \\ A & n = m \\ \rho^{|m-n-1|} A_{12}^* & n > m \end{cases} .$$

R_s is then completely specified once A , A_{12} , and ρ are known.

A and A_{12} are also completely specified once P , K , ρ_s , and

$R_x(0)$ are known.

4.3 Evaluation Procedures

The procedures used in evaluating the performance are presented and expressions for performance characterization are

derived. The block diagram of the optimum detector is repeated below. The techniques used in performance evaluation and characterization only require knowledge of the eigenvalues, λ_n .

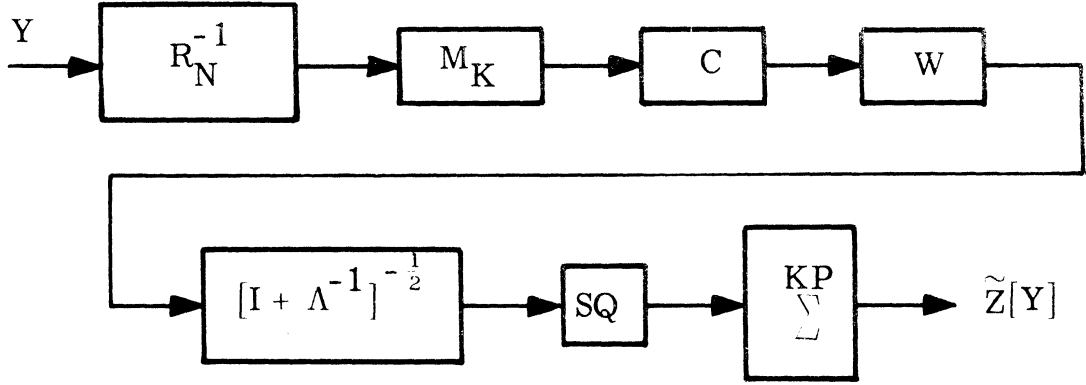


Fig. 3.4. Optimum detector for WSCS processes

4.3.1 ROC Generation. Given the statistics of $\tilde{Z}[Y]$ under H_0 and H_1 , $f[\tilde{Z}[Y]|H_0]$ and $f[\tilde{Z}[Y]|H_1]$, the probability of detection, P_D , and the probability of false alarm, P_{FA} , are (see Section 2.1.2)

$$P_D = \int_c^\infty f[\tilde{Z}[Y]|H_1] d\tilde{Z} \quad (4.1)$$

and

$$P_{FA} = \int_c^\infty f[\tilde{Z}[Y]|H_0] d\tilde{Z} . \quad (4.2)$$

The ROC's will only be generated for the ROC evaluation region.

The ROC evaluation region is either that region of the ROC where

$$0.01 \leq P_D \leq 0.99$$

and

$$0.01 \leq P_{FA} \leq 0.9 ,$$

or is that region of $f[\tilde{Z}[Y] H_0]$ and $f[\tilde{Z}[Y] H_1]$ such that when $f[\tilde{Z}[Y] H_0]$ and $f[\tilde{Z}[Y] H_1]$ are substituted in Eqs. 4.1 and 4.2

$$0.01 \leq P_D \leq 0.99$$

and

$$0.01 \leq P_{FA} \leq 0.9 .$$

The exact meaning will be clear by the context.

It was shown in Section 3.3 that the KP dimensional vector V ,

$$V = W C M R_N^{-1} Y ,$$

is a zero mean Gaussian vector with independent components, Eq.

3.11. It then follows, that the correlation matrix of V' , $R_{V'}$, where

$$V' = [I + \Lambda^{-1}]^{-\frac{1}{2}} V$$

is

$$\mathbf{R}_{\mathbf{V}'} = \begin{cases} \Lambda^{-1} [\mathbf{I} + \Lambda^{-1}]^{-1}, & H_0 \\ \Lambda^{-1} & H_1 \end{cases} . \quad (4.3)$$

Consequently under H_0 and H_1 , $\tilde{\mathbf{Z}}|\mathbf{Y}$ is the sum of the squares of independent Gaussian random variables with different variances where the variances are the diagonal elements of $\mathbf{R}_{\mathbf{V}'}$. $f[\tilde{\mathbf{Z}}|\mathbf{Y}|H_0]$ and $f[\tilde{\mathbf{Z}}|\mathbf{Y}|H_1]$ are obtained by taking the inverse Fourier Transform of the characteristic function under H_0 and H_1 and integrating as in Eqs. 4.1 and 4.2. See Section 2.2 for more details on the procedure.

4.3.2 Input Signal-to-Noise Ratio. The input signal-to-noise ratio, $\text{SNR}_{\mathbf{I}}$, is a meaningful measure of the amount of signal relative to the amount of noise. Let the diagonal elements of the signal and noise correlation matrices be respectively $r_{\mathbf{S}}(n)$ and $r_{\mathbf{N}}(n)$ for $n = 1, 2, 3, \dots, \text{KP}$. $\text{SNR}_{\mathbf{I}}$ is defined as

$$\text{SNR}_{\mathbf{I}} = \frac{\frac{1}{\text{KP}} \sum_{n=1}^{\text{KP}} r_{\mathbf{S}}(n)}{\frac{1}{\text{KP}} \sum_{n=1}^{\text{KP}} r_{\mathbf{N}}(n)} . \quad (4.4)$$

For the noise model under consideration

$$r_{\mathbf{N}}(n) = N_0 .$$

Therefore

$$\frac{1}{\text{KP}} \sum_{n=1}^{\text{KP}} r_N^{(n)} = N_0 \quad (4.5)$$

Substitute Eq. 4.5 into Eq. 4.4. Then

$$\begin{aligned} \text{SNR}_I &= \frac{1}{\text{KP}} \sum_{n=1}^{\text{KP}} \frac{r_S^{(n)}}{N_0} \\ &= \frac{1}{\text{KP}} \text{TR}[\mathbf{R}_S \mathbf{R}_N^{-1}] \end{aligned}$$

where $\text{TR}[\]$ is the trace of the matrix in brackets. It is shown in Appendix A that

$$\text{TR}[\mathbf{R}_S \mathbf{R}_N^{-1}] = \sum_{n=1}^{\text{KP}} \lambda_n^{-1}$$

where the λ_n are the eigenvalues. It then follows that

$$\text{SNR}_I = \frac{1}{\text{KP}} \sum_{n=1}^{\text{KP}} \lambda_n^{-1} .$$

4.3.3 Detectability Index. A meaningful measure of the detector performance is the point where the ROC curves cross the negative diagonal, $P_{\text{FA}} + P_{\text{D}} = 1$. The detectability index, d' , is the measure of that crossing point and is easily calculated for a normal ROC.

Assume that the ROC for the optimum detector is normal or can be closely approximated by a normal ROC. d' is then defined

as (Ref. 2)

$$d' = \sqrt{\frac{E[\tilde{Z}[Y]|H_1] - E[\tilde{Z}[Y]|H_0]}{2}}. \quad (4.6)$$

It is seen that, Section 4.3.1,

$$E[\tilde{Z}[Y]|\cdot] = \begin{cases} \sum_{n=1}^{KP} \lambda_n^{-1} (1 + \lambda_n^{-1})^{-1}, & H_0 \\ \sum_{n=1}^{KP} \lambda_n^{-1}, & H_1 \end{cases}. \quad (4.7)$$

$$\sum_{n=1}^{KP} \lambda_n^{-1}, \quad H_1 \quad (4.8)$$

Substitute Eqs. 4.7 and 4.8 into Eq. 4.6. Then

$$d' = \sqrt{\frac{1}{2} \sum_{n=1}^{KP} [\lambda_n^{-2} (1 + \lambda_n^{-1})]^{-1}}. \quad (4.9)$$

The eigenvalues are initially calculated for a SNR_I of unity because any other SNR_I can be obtained by multiplying the eigenvalues by a constant. The performance is obtained for the detectability indices of 0.25, 0.5, 1.0, and 1.5. β is set at 0.0625 so as not to sample at the zeroes of $\cos 2\pi f_0 t$. The eigenvalue multiplicative modifying constant is found by the Newton-Raphson method used to search for the stated d' , and the SNR_I follows from the new eigenvalues.

4.4 Performance

The ROC's and performance data are presented and discussed followed by specific conclusions.

It is observed, in the ROC evaluation region, that the ROC's are binormal. This only indicates that the optimum ROC's behave as binormal ROC's in the ROC evaluation region. See Section 2.1.4 for more details on binormal ROC's.

Six representative ROC's are presented in Figs. 4.1 to 4.6. Since a binormal ROC curve can be parameterized by two parameters, the slope and detectability index, the optimum ROC's are summarized in Table 4.1. The parameters listed in Table 4.1 are defined below.

K:	number of periods in an observation
P:	number of samples in a period
ρ :	period-to-period correlation coefficient, $\rho = \rho_S^P$
ρ_S :	sample-to-sample correlation coefficient
d' :	desired detectability index
d_e' :	actual detectability index
SNR_I :	input signal-to-noise ratio
SLOPE:	slope of the ROC curve

For a binormal ROC (see Appendix C),

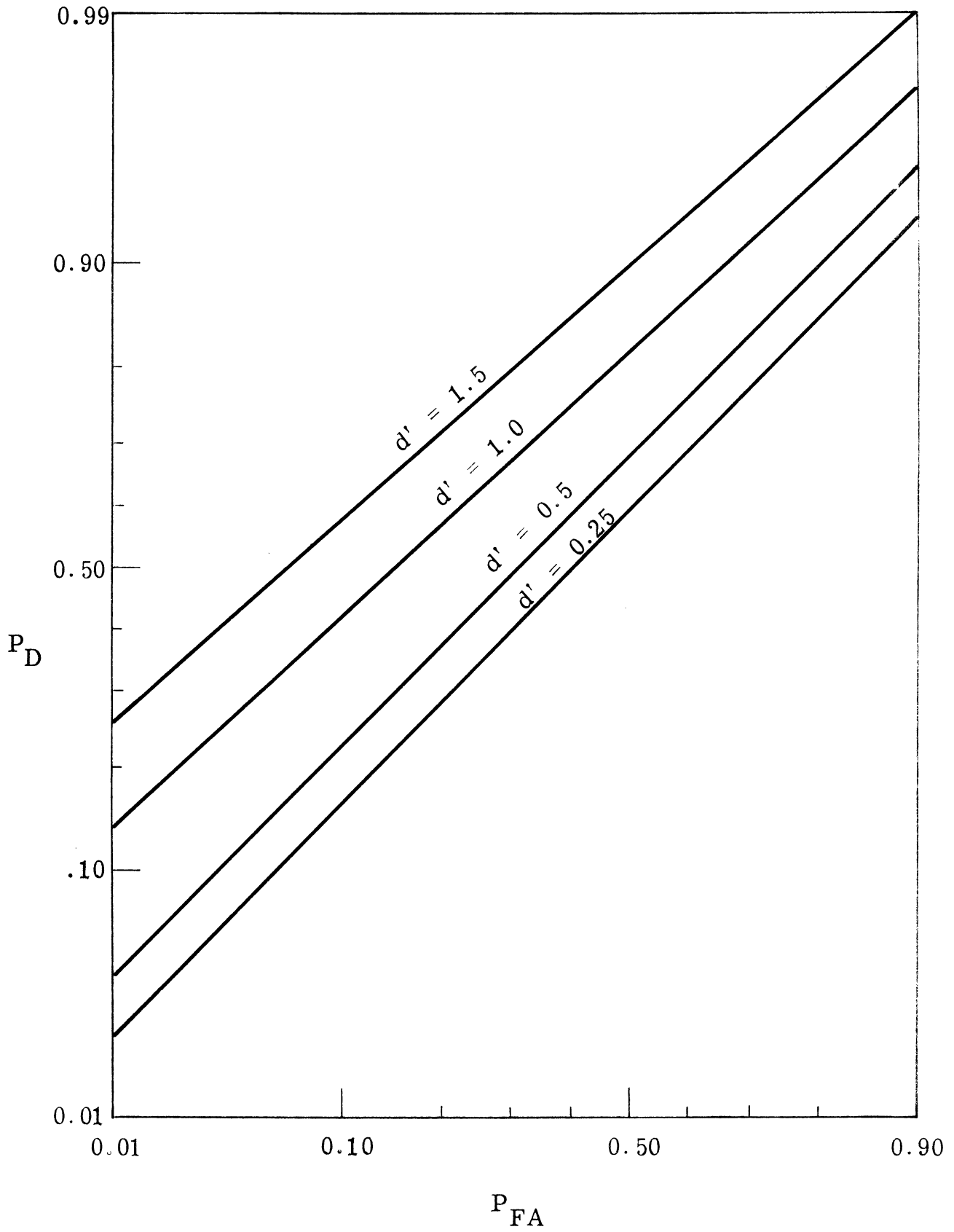


Fig. 4.1. ROC curves for optimum detector for
 $K = 4$, $P = 4$, $\rho_S = 0.25$

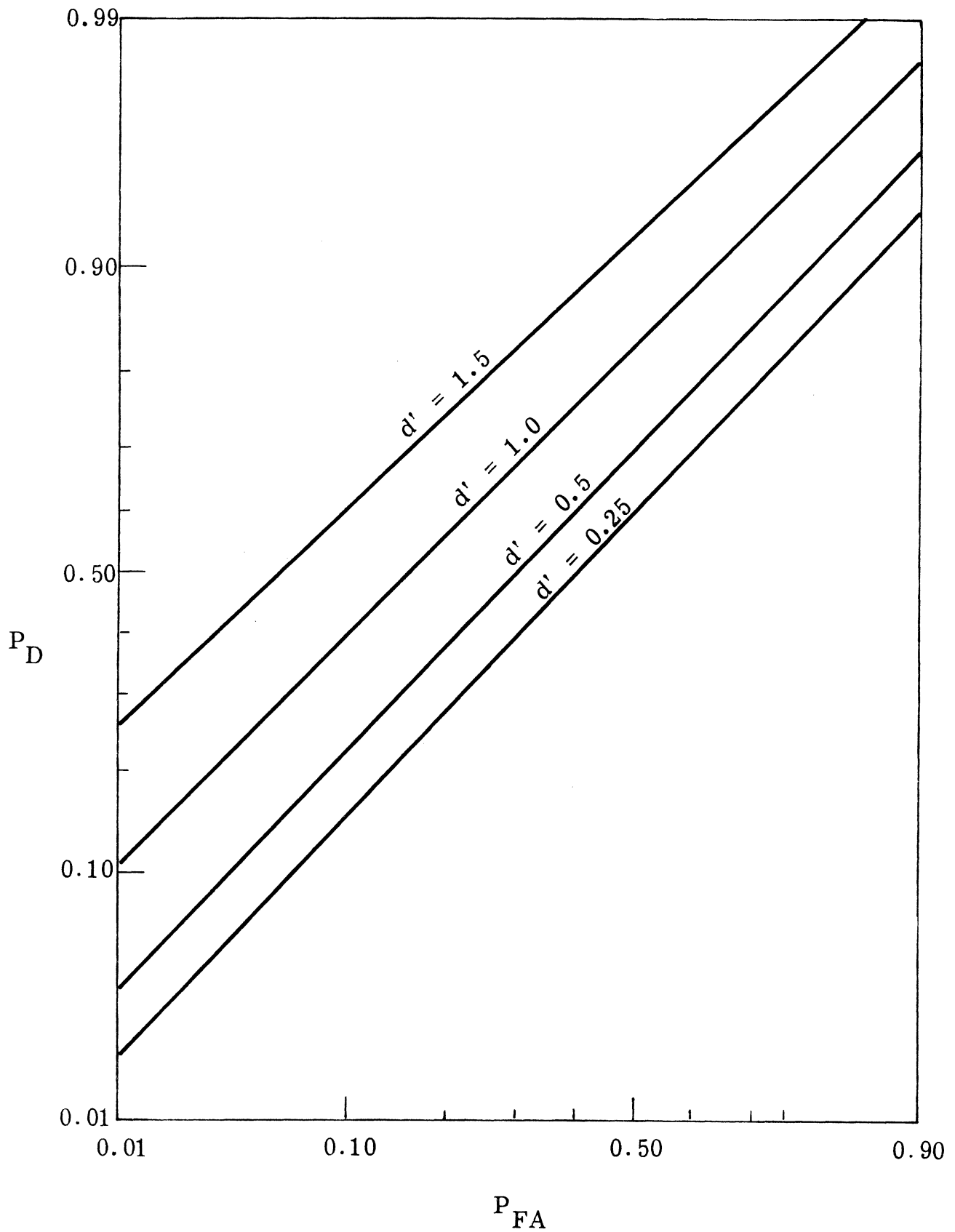


Fig. 4.2. ROC curves for optimum detector for $K = 16$, $P = 4$, $\rho_S = 0.25$

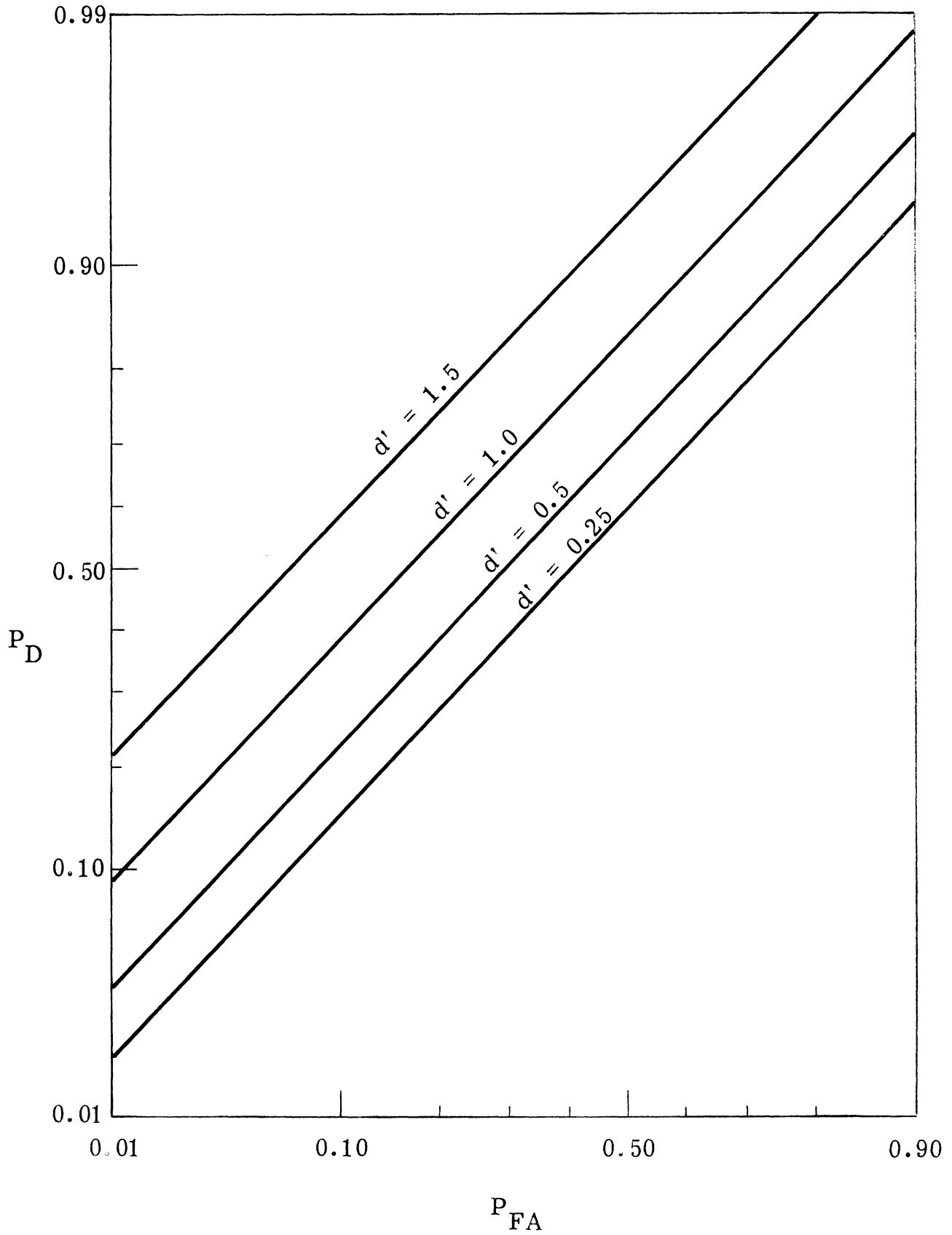


Fig. 4.3. ROC curves for optimum detector for $K = 64$, $P = 4$, $\rho_s = 0.25$

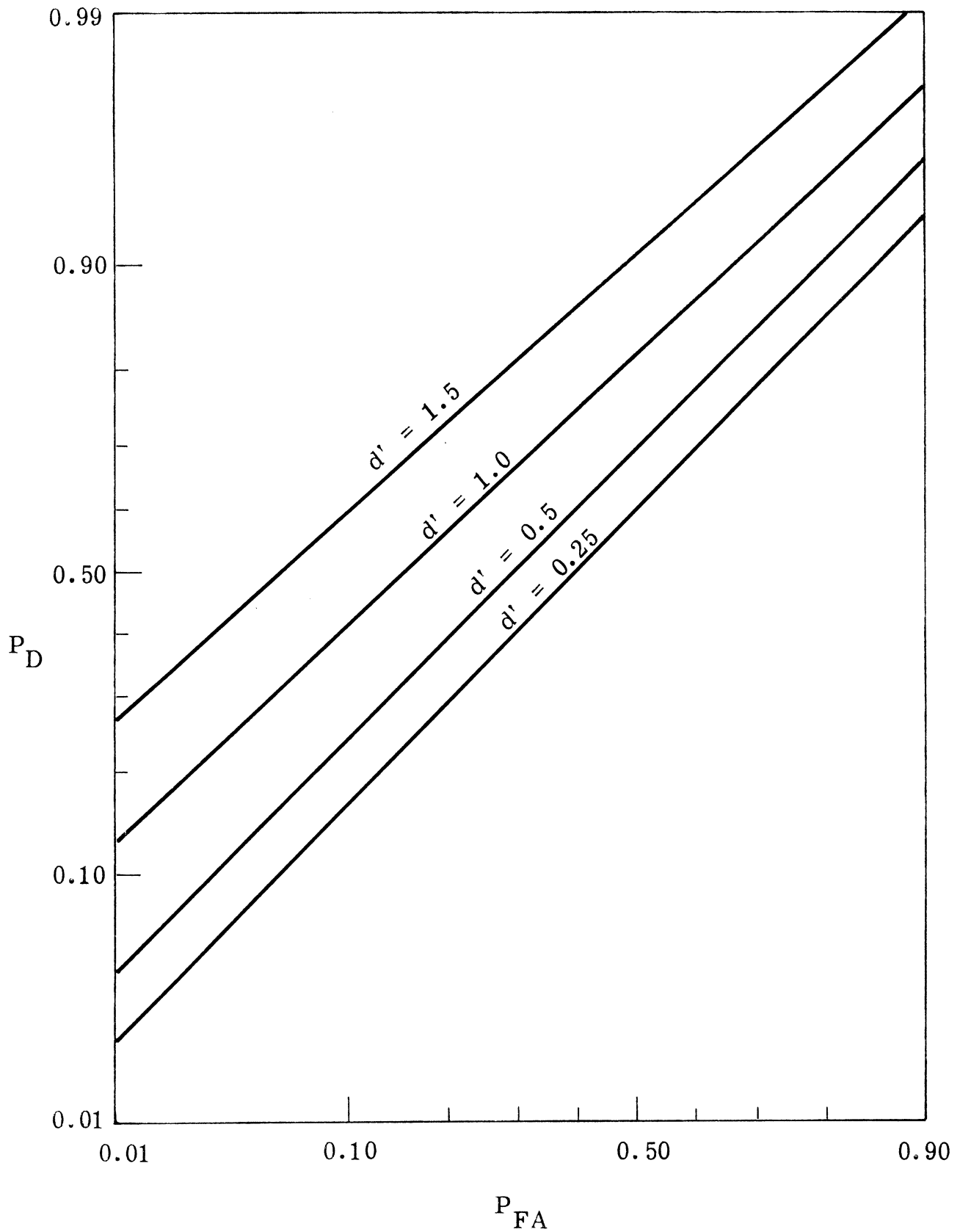


Fig. 4.4. ROC curves for optimum detector for
 $K = 1$, $P = 16$, $\rho_S = 0.707$

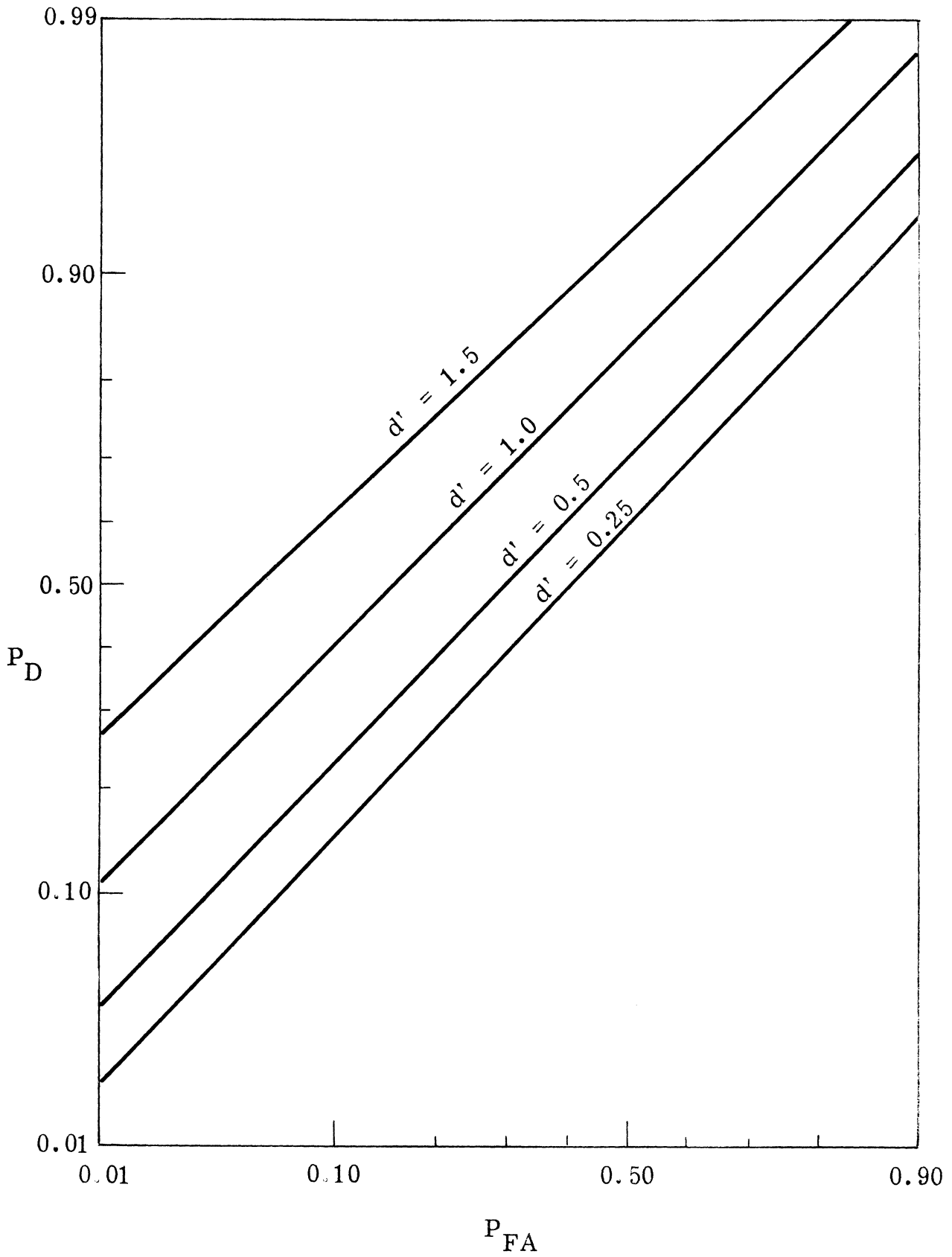


Fig. 4.5. ROC curves for optimum detector for $K = 4$, $P = 16$, $\rho_S = 0.707$

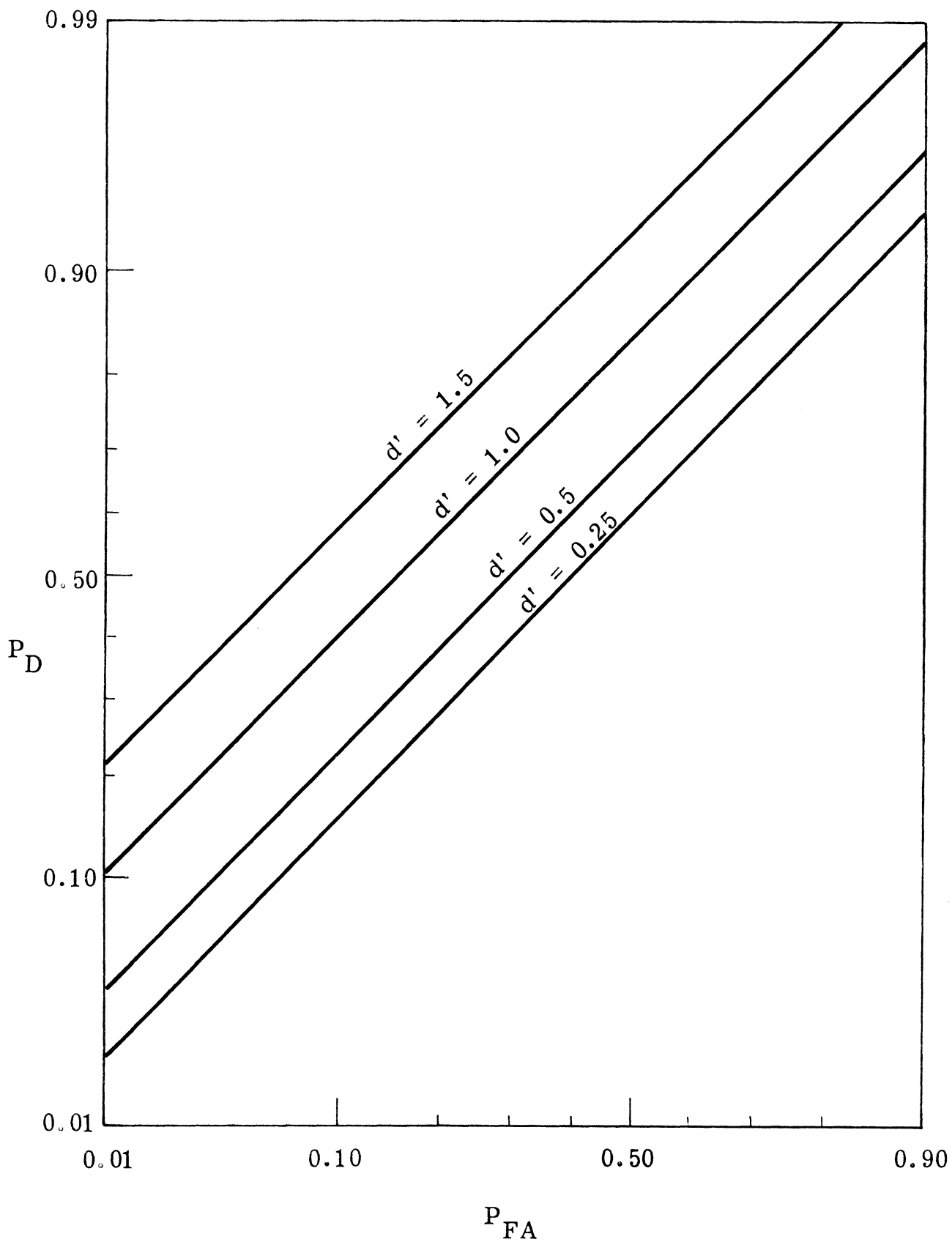


Fig. 4.6. ROC curves for optimum detector for
 $K = 16$, $P = 16$, $\rho_s = 0.707$

$$d_e' = \frac{2(m_1 - m_0)}{\sigma_1 + \sigma_0} , \quad (2.11)$$

and

$$\text{SLOPE} = \sigma_0 / \sigma_1 \quad (2.12)$$

where

1. m_0 is the mean of $\tilde{Z}[Y]$ under H_0 ,
2. m_1 is the mean of $\tilde{Z}[Y]$ under H_1 ,
3. σ_0^2 is the variance of $\tilde{Z}[Y]$ under H_0 ,
4. σ_1^2 is the variance of $\tilde{Z}[Y]$ under H_1 .

It is seen that the slope is a measure of the differences in the variance of and d_e' is a measure of the difference in the mean of $\tilde{Z}[Y]$ under H_0 and H_1 . The relationships between the various parameters in Table 4.1 are plotted in Figs. 4.7-4.9 for a representative example as an aid in interpreting Table 4.1.

It is seen from Table 4.1 and Fig. 4.7 that for a given K , P , ρ the ROC is normal for low d' and d_e' equals d' . However as d' increases, the ROC deviates from the normal and d_e' becomes smaller than d' for small K and is approximately d' for large K . This is due to the degree of similarity between $f[\tilde{Z}[Y] | H_0]$ and $f[\tilde{Z}[Y] | H_1]$ in the ROC evaluation region.

The variance of $\tilde{Z}[Y]$ under H_0 and H_1 are approximately

K	P	ρ	ρ_s	$d' = 0.25$			$d' = 0.5$			$d' = 1.0$			$d' = 1.5$		
				d'_e	SNR _I	SLOPE	d'_e	SNR _I	SLOPE	d'_e	SNR _I	SLOPE	d'_e	SNR _I	SLOPE
4	4	0.250	0.707	0.25	0.059	1.000	0.50	0.128	0.980	0.97	0.300	0.860	1.42	0.520	0.854
16	4	0.250	0.707	0.25	0.028	1.000	0.51	0.059	1.000	1.03	0.130	0.921	1.50	0.210	0.880
64	4	0.250	0.707	0.25	0.014	1.000	0.50	0.028	1.000	1.00	0.058	0.990	1.50	0.091	0.954
4	4	0.00391	0.250	0.25	0.068	1.000	0.50	0.146	0.980	0.98	0.331	0.890	1.41	0.559	0.860
16	4	0.00391	0.250	0.25	0.033	1.000	0.50	0.069	1.000	0.98	0.146	0.940	1.50	0.234	0.905
64	4	0.00391	0.250	0.25	0.016	1.000	0.55	0.033	1.000	1.00	0.069	0.990	1.50	0.106	0.991
1	16	0.00390	0.707	0.25	0.055	1.000	0.50	0.121	0.980	0.91	0.290	0.851	1.39	0.512	0.784
4	16	0.00390	0.707	0.26	0.026	1.000	0.50	0.055	1.000	1.00	0.121	0.911	1.41	0.199	0.905
16	16	0.00390	0.707	0.25	0.013	1.000	0.51	0.026	1.000	1.00	0.055	0.931	1.50	0.086	0.924
1	16	2.33×10^{-10}	0.250	0.25	0.074	1.000	0.50	0.157	1.000	0.97	0.356	0.860	1.45	0.599	0.829
4	16	2.33×10^{-10}	0.250	0.25	0.036	1.000	0.52	0.074	1.000	1.00	0.157	0.990	1.55	0.251	0.954
16	16	2.33×10^{-10}	0.250	0.25	0.018	1.000	0.51	0.036	1.000	1.10	0.074	0.990	1.49	0.114	0.965
1	16	0.250	0.917	0.25	0.038	1.000	0.48	0.087	0.890	0.88	0.225	0.815	1.13	0.420	0.730
4	4	0.707	0.917	0.25	0.039	1.000	0.48	0.090	0.927	0.85	0.232	0.806	1.14	0.430	0.826
1	16	0.707	0.979	0.25	0.030	1.000	0.48	0.070	0.930	0.85	0.189	0.800	1.10	0.366	0.666

Table 4.1. Summary of optimum detector performance

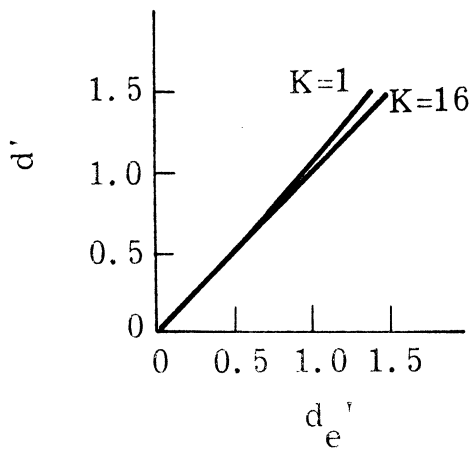
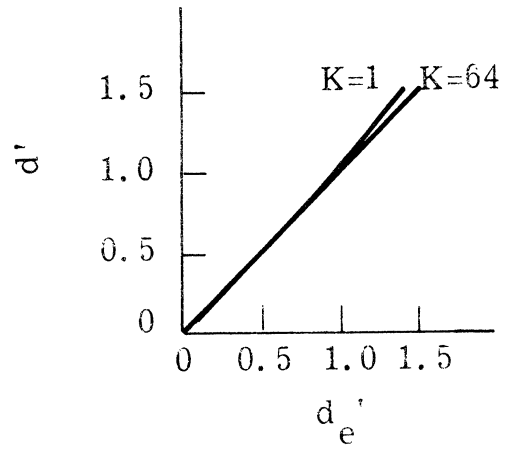
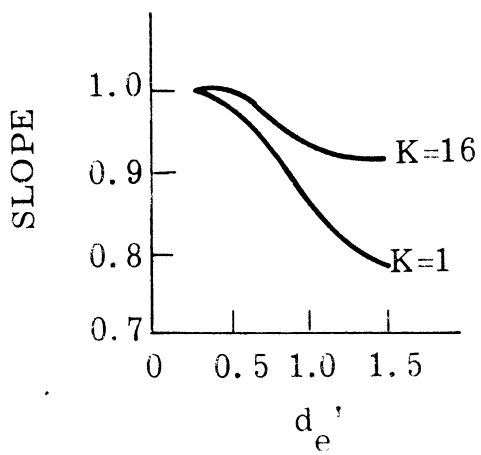
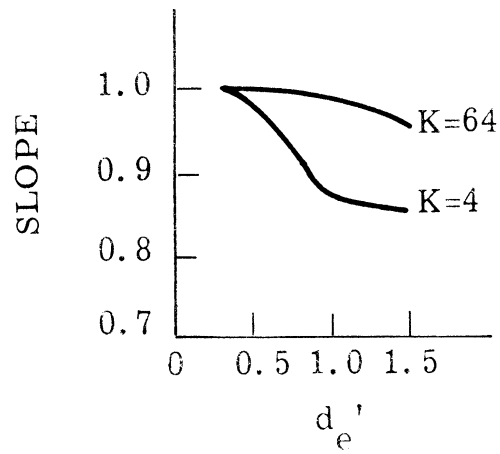
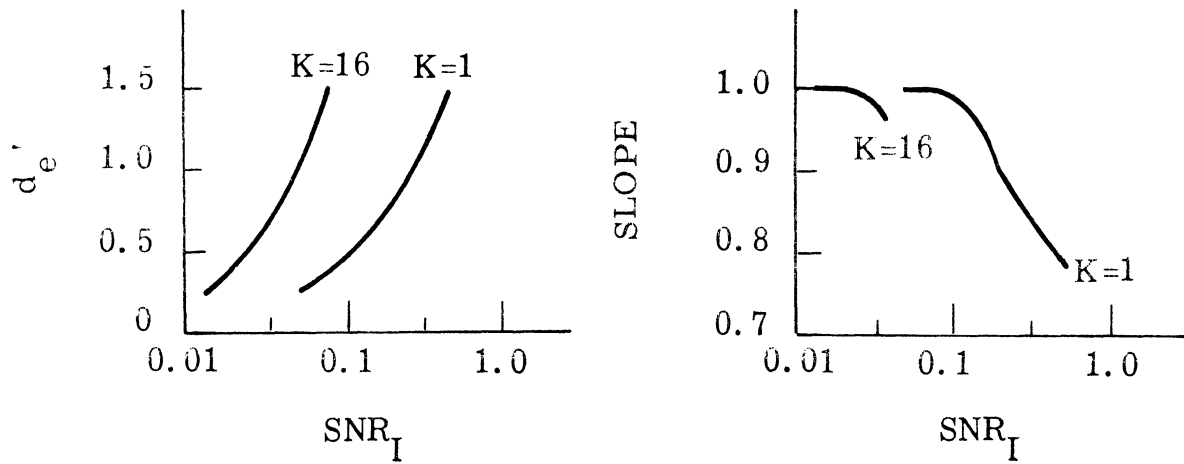
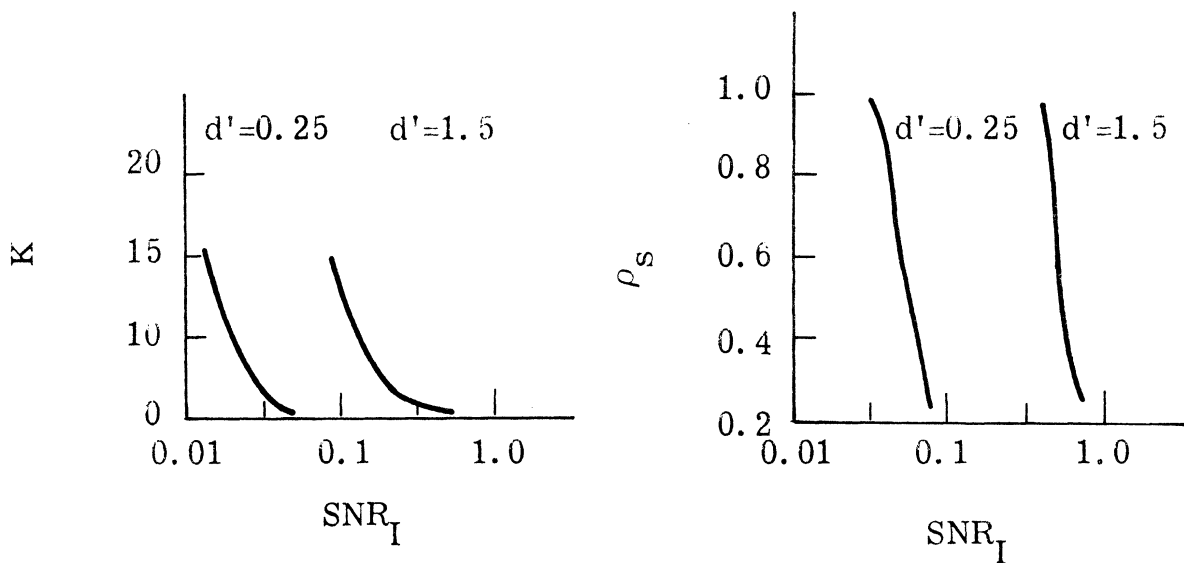
(a) d' vs. d_e' for $P = 16$ (b) d' vs. d_e' for $P = 4$ (c) SLOPE vs. d_e' for $P = 16$ (d) SLOPE vs. d_e' for $P = 4$

Fig. 4.7. Performance summary of the optimum detector as a function of d_e' for $\rho_S = 0.707$

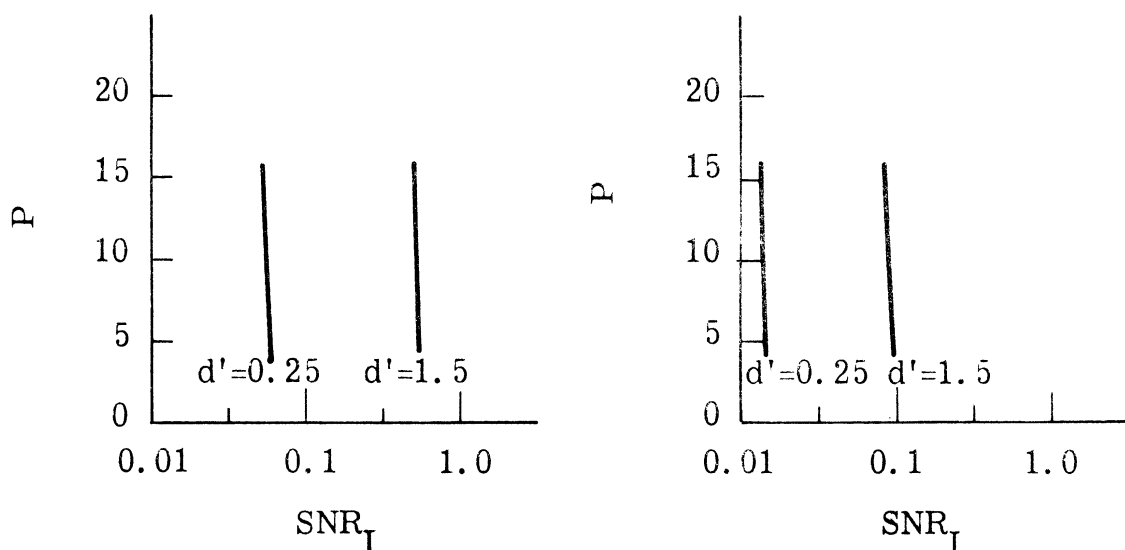


(a) d'_e vs. SNR_I for $\rho_S = 0.707$ (b) SLOPE vs. SNR_I for $\rho_S = 0.707$



(c) K vs. SNR_I for $\rho_S = 0.707$ (d) ρ_S vs. SNR_I for $K = 1$

Fig. 4.8. Performance summary of the optimum detector as a function of SNR_I for $P = 16$



(a) P vs. SNR_I for $KP = 16$ (b) P vs. SNR_I for $KP = 256$

Fig. 4.9. P as a function of SNR_I for $\rho_s = 0.707$

equal, and the ROC is approximately normal for low SNR_I (Figs. 4.8a and 4.8b). However as SNR_I increases, the variance of $\tilde{Z}[Y]$ under H_0 and H_1 begin to differ more, and the ROC becomes less normal. The fact that the ROC is binormal indicates that $f[\tilde{Z}[Y] | H_0]$ and $f[\tilde{Z}[Y] | H_1]$ behave approximately as Gaussian probability density functions in the ROC evaluation region.

The degree of similarity between $f[\tilde{Z}[Y] | H_0]$ and $f[\tilde{Z}[Y] | H_1]$ decreases as ρ or ρ_s increases for a given P and any K (Figs. 4.8b and 4.8d). This is due to an increasing difference between the detector input statistics under H_0 and H_1 . Some of this effect can be reduced by increasing K but the value of ρ or

ρ_s is the controlling factor.

The SNR_I required for any d' decreases as the observation time (KP) increases for constant ρ or ρ_s and constant period (P). This is expected and is a result of the integrating filter (Fig. 4.8c).

The SNR_I required for any d' decreases as ρ or ρ_s increase for a constant period (P) and a constant observation time (KP). This is a result of the increasing statistical difference between H_0 and H_1 as ρ or ρ_s increase (Fig. 4.8d).

The SNR_I required for any d' decreases as the period (P) is increased for a constant observation time (KP) and a constant ρ or ρ_s (Fig. 4.9). This decrease in required SNR_I is slight but does indicate a trend.

The performance results indicate that the only ways to reduce the required SNR_I for a given d' is to increase ρ or ρ_s , P, K, or any combination thereof. One usually has no control over the parameters ρ , ρ_s , and P. Consequently the only way to improve performance is to increase KP by increasing K.

It should be observed that for the signal model selected indicates that increasing the sampling rate to increase ρ or ρ_s and P improves performance. The signal model further allows for a never ending increase in sampling rate. This is a result of the infinite bandwidth of the signal $s(t)$. In actuality signals have finite

bandwidth. Consequently increasing the sampling rate over the Nyquist rate may improve the performance slightly. However increasing K will improve the performance much more than increasing the sampling rate. This is a consequence of the fact that once a CS process is specified, P and ρ are usually fixed.

4.5 Summary

Performance results are derived for a real zero mean WSCS Gauss-Markov process with period P . The autocorrelation matrix for this process is completely specified once the autocorrelation matrix for any period (A), the correlation matrix between adjacent period (A_{12}), and the period-to-period correlation coefficient (ρ) are known.

It is found that the required SNR_1 for a d' can be reduced by increasing the sample-to-sample correlation coefficient (ρ_s) or the period-to-period correlation coefficient (ρ), the size of the period (P), and the number of period observed. It is noted that in actuality the Nyquist sampling rate imposes a severe limitation on the control one has over ρ or ρ_s and P by varying the sampling rate. Once a WSCS process is specified, P and ρ or ρ_s are specified and improving performance is limited to increasing the observation time (KP).

CHAPTER V

A SUBOPTIMUM DETECTOR

5.1 Introduction

An optimum detector was derived in Chapter III, and its performance evaluated in Chapter IV. A suboptimum detector that performs almost as well as and is easier to implement than the optimum detector is highly desirable. It is usually a suboptimum detector that is implemented in practice.

The suboptimum detector is derived. Its approximate performance for the signal model presented in Chapter IV is evaluated and compared to the optimum performance.

5.2 Suboptimum Detector

The block diagram of the optimum detector is repeated below in Fig. 3.4. It was shown in Section 3.4.1 that the weighting filter,

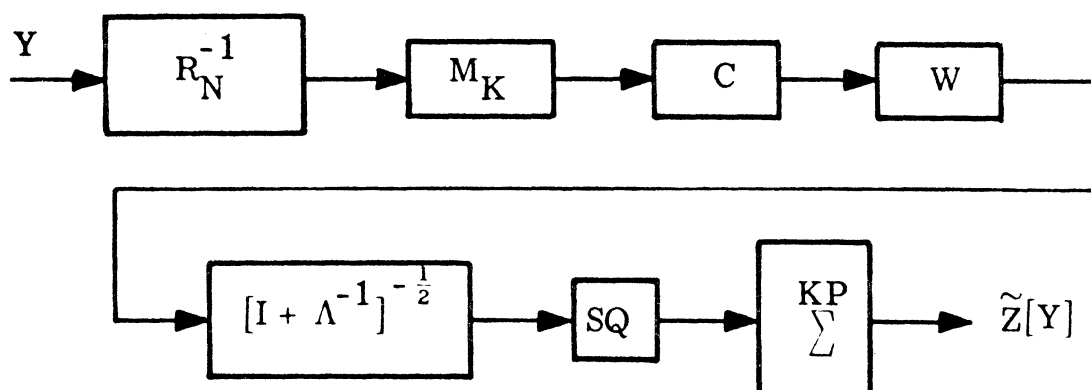


Fig. 3.4. Optimum detector for WSCS processes

$[\mathbf{I} + \Lambda^{-1}]^{-\frac{1}{2}}$, approaches the identity filter, \mathbf{I} , for small SNR_I 's.

The weighting filter modifies the optimum structure for departures from the small SNR_I case.

The small SNR_I form of the optimum detector is the suboptimum detector studied and is shown in Fig. 5.1. $\tilde{Z}_s[Y]$ is the suboptimum decision variable. The suboptimum detector is expected to perform as well as the optimum detector for small SNR_I . It is also expected that the suboptimum performance is close to the optimum performance for large SNR_I . For large SNR_I , the signal is easily detected, and the exact detector structure should not be critical.

It was shown in Section 3.3 that V is a Gaussian vector with independent components under H_0 and H_1 , Eq. 3.11, where

$$V = W C M R_N^{-1} Y .$$

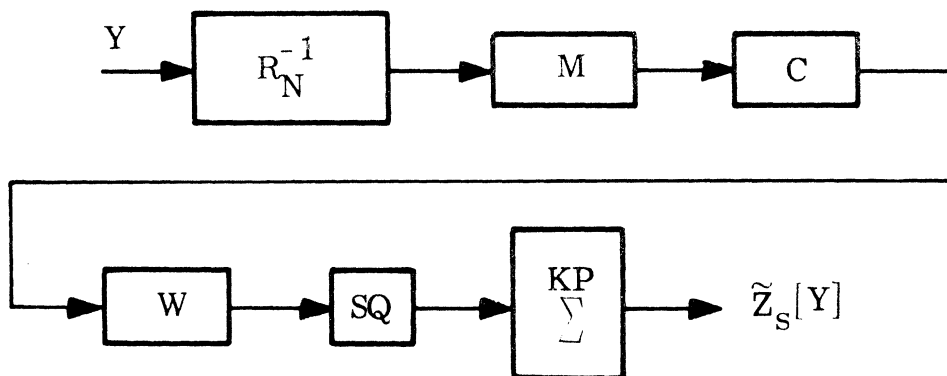


Fig. 5.1. A suboptimum detector for WSCS processes

Consequently $\tilde{Z}_s[Y]$ is the sum of squares of independent Gaussian random variables under H_0 and H_1 . It follows that the mean and variance of $\tilde{Z}_s[Y]$ under H_0 and H_1 are

$$\text{mean} = \begin{cases} \sum_{n=1}^{KP} \lambda_n^{-1} & , \quad H_0 \\ \sum_{n=1}^{KP} \lambda_n^{-1} [1 + \lambda_n^{-1}] & , \quad H_1 \end{cases} \quad (5.1)$$

and

$$\text{variance} = \begin{cases} 2 \sum_{n=1}^{KP} \lambda_n^{-2} [1 + \lambda_n^{-1}]^2 & , \quad H_0 \\ 2 \sum_{n=1}^{KP} \lambda_n^{-2} & , \quad H_1 \end{cases} \quad (5.2)$$

5.3 Evaluation Procedures

The ability to parameterize the suboptimum ROC in the ROC evaluation region by one or two parameters is highly desirable. This would facilitate the comparison between the optimum and suboptimum performance.

According to the Central Limit Theorem, $f[\tilde{Z}_s[Y] | H_0]$ and $f[\tilde{Z}_s[Y] | H_1]$ may be approximated by the normal density function with means and variances as in Eqs. 5.1 and 5.2. Consequently the approximation to the suboptimum ROC in the ROC evaluation region

will be a binormal ROC. This approximation is further supported by the fact that the optimum ROC is binormal in the ROC evaluation region. The approximate suboptimum ROC can then be parameterized by a d_{es}' and a $SLOPE_S$.

The d_{es}' , and $SLOPE_S$ for a binormal ROC were derived in Appendix C, explained in Chapter II, and are repeated below.

$$d_{es}' = \frac{2(m_1 - m_0)}{\sigma_1 + \sigma_0} \quad (2.11)$$

and

$$SLOPE_S = \sigma_0/\sigma_1 \quad (2.12)$$

where

1. m_0 is the mean of $\tilde{Z}_S[Y]$ under H_0 .
2. m_1 is the mean of $\tilde{Z}_S[Y]$ under H_1 .
3. σ_0^2 is variance of $\tilde{Z}_S[Y]$ under H_0 .
4. σ_1^2 is the variance of $\tilde{Z}_S[Y]$ under H_1 .

The approximate suboptimum performance is then easily calculated given m_0 , m_1 , σ_0 , and σ_1 for the SNR_I 's and detectability indices used in optimum performance calculations.

5.4 Performance

The suboptimum performance will be compared with the optimum performance in two ways. The first comparison will be the

statistics of the optimum and suboptimum decision variables under H_0 and H_1 . This comparison will indicate the stability of the optimum and suboptimum statistics and has a strong bearing on the second comparison. The second comparison will be the optimum and suboptimum ROC's.

5.4.1 Decision Variable Statistics. The means and variances of $\tilde{Z}_s[Y]$ are listed in Eqs. 5.1 and 5.2. The means and variances of $\tilde{Z}[Y]$ are easily calculated, Eq. 4.3, and are listed below.

$$\text{mean} = \begin{cases} \sum_{n=1}^{KP} \lambda_n^{-1} [1 + \lambda_n^{-1}]^{-1}, & H_0 \\ \sum_{n=1}^{KP} \lambda_n^{-1}, & H_1 \end{cases}, \quad (5.3)$$

and

$$\text{variance} = \begin{cases} 2 \sum_{n=1}^{KP} \lambda_n^{-2} [1 + \lambda_n^{-1}]^{-2}, & H_0 \\ 2 \sum_{n=1}^{KP} \lambda_n^{-2}, & H_1 \end{cases}. \quad (5.4)$$

It is seen that the terms in the expressions for the statistics of $\tilde{Z}[Y]$ and $\tilde{Z}_s[Y]$ vary differently with the eigenvector

signal-to-noise ratio. The different manners in which the terms vary with the eigenvector signal-to-noise ratio are listed below.

$$\text{optimum mean } \alpha \begin{cases} x(1+x)^{-1}, & H_0 \\ x, & H_1 \end{cases} \quad (5.5)$$

$$\text{optimum variance } \alpha \begin{cases} x^2(1+x)^{-2}, & H_0 \\ x^2, & H_1 \end{cases} \quad (5.6)$$

$$\text{suboptimum mean } \alpha \begin{cases} x, & H_0 \\ x(1+x), & H_1 \end{cases} \quad (5.7)$$

and

$$\text{suboptimum variance } \alpha \begin{cases} x^2, & H_0 \\ x^2(1+x)^2, & H_1 \end{cases} \quad (5.8)$$

where

1. α is read "proportional to".
2. x is the eigenvector signal-to-noise ratio, λ_n^{-1} .

The expressions in Eqs. 5.5 to 5.8 are plotted in Fig. 5.2. It is seen that the optimum statistics are unbounded under H_1 and bounded under H_0 . This is a desirable feature because the statistics under H_0 do not increase unboundly as the signal power is increased.

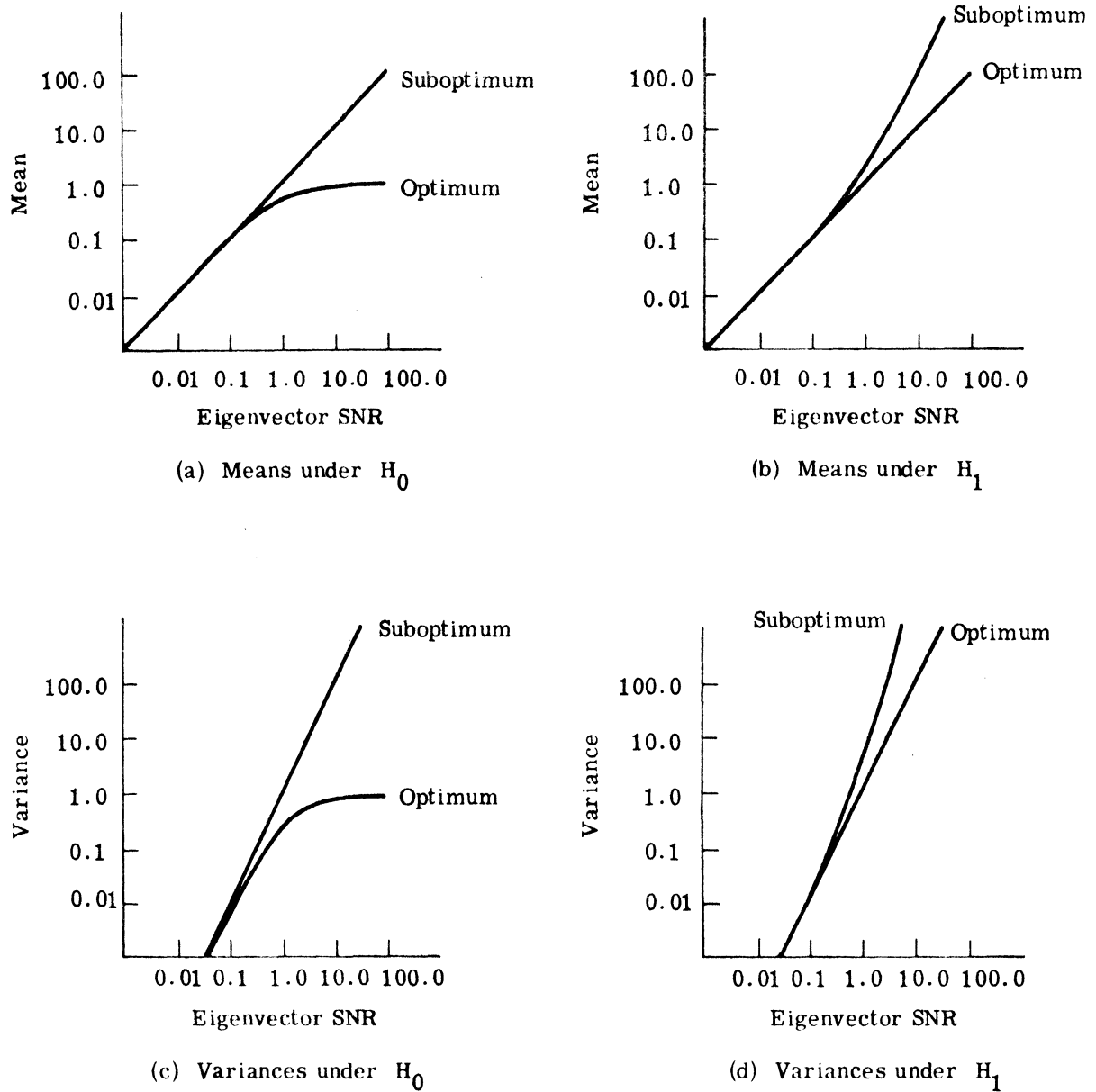


Fig. 5.2. Behavior of the terms in the expressions for the mean and variance of the optimum and suboptimum decision variables under H_0 and H_1

For low to moderate SNR_I , the optimum statistics under H_0 and H_1 increase linearly with SNR_I . This accounts for the fact that $f[\tilde{Z}[Y]|H_0]$ and $f[\tilde{Z}[Y]|H_1]$ are similar; and consequently the SLOPE is unity, and $d_e' = d'$ for low to moderate SNR_I . However as SNR_I increases, $f[\tilde{Z}[Y]|H_0]$ doesn't change but $f[\tilde{Z}[Y]|H_1]$ continuously changes. This explains the decreasing SLOPE and d_e' for increasingly large SNR_I .

The suboptimum statistics are unbounded under H_0 and H_1 . This is undesirable because the statistics under H_0 increase unboundedly as signal power increases. It is seen that under H_1 the suboptimum statistics vary nonlinearly with SNR_I while the suboptimum statistics vary linearly with SNR_I under H_0 . This indicates that for low SNR_I , $f[\tilde{Z}_s[Y]|H_0]$ and $f[\tilde{Z}_s[Y]|H_1]$ are similar. However for moderate and large SNR_I , the difference between $f[\tilde{Z}_s[Y]|H_0]$ and $f[\tilde{Z}_s[Y]|H_1]$ increases nonlinearly with SNR_I .

On the basis of statistic stability, the optimum detector is more desirable than the suboptimum detector. This is unexpected. The usual case is for the suboptimum detector to have more stable statistics than the optimum detector which is tuned to the exact statistics of the input.

5.4.2 ROC Comparison. The suboptimum ROC data is summarized in Table 5.1 for the binormal approximation in the ROC evaluation region. The suboptimum ROC data is calculated with the eigenvalues obtained for evaluating the optimum performance. The

parameters listed in Table 5.1 are defined below.

K:	number of periods in an observation
P:	number of samples in a period
ρ :	period-to-period correlation coefficient, $\rho = \rho_s^P$
ρ_s :	sample-to-sample correlation coefficient
d' :	desired detectability index
d_{es}' :	actual suboptimum detectability index
SNR_I :	input signal-to-noise ratio
$SLOPE_s$:	slope of the suboptimum ROC curve.

The relationships between the various parameters in Table 5.1 are plotted in Figs. 5.3-5.5 for the representative example used in Figs. 4.7-4.9 as an aid in interpreting Table 5.1.

It is seen, by comparing Tables 4.1 and 5.1, that the relationships between $SLOPE$, K , P , d' , d_e' , and SNR_I are the same for the optimum and suboptimum detectors (compare Figs. 4.7 and 5.3 and Figs. 4.8 and 5.4).

For small SNR_I , $d_{es}' = d'$ which is expected because the suboptimum detector is the small SNR_I form of the optimum detector (compare Figs. 4.8a and 5.4b). However the divergence of d_{es}' from d' for moderate to large SNR_I is larger than the divergence of d_e' from d' . Simultaneously $SLOPE_s$ is always less than $SLOPE$ and $SLOPE_s$ respectively for increasing SNR_I is due to the instability of the suboptimum statistics.

K	P	ρ	ρ_s	$d' = 0.25$			$d' = 0.5$			$d' = 1.0$			$d' = 1.5$		
				d'_{es}	SNR_I	SLOPE _s	d'_{es}	SNR_I	SLOPE _s	d'_{es}	SNR_I	SLOPE _s	d'_{es}	SNR_I	SLOPE _s
4	4	0.250	0.707	0.25	0.059	0.836	0.50	0.128	0.700	0.92	0.300	0.496	1.27	0.520	0.361
16	4	0.250	0.707	0.25	0.028	0.914	0.50	0.059	0.830	0.97	0.130	0.690	1.42	0.210	0.576
64	4	0.250	0.707	0.25	0.014	0.954	0.50	0.028	0.911	0.99	0.058	0.830	1.48	0.091	0.758
4	4	0.00391	0.250	0.25	0.068	0.882	0.50	0.146	0.778	0.97	0.331	0.608	1.40	0.559	0.479
16	4	0.00391	0.250	0.25	0.033	0.939	0.50	0.069	0.882	0.99	0.146	0.778	1.47	0.234	0.687
64	4	0.00391	0.250	0.25	0.016	0.969	0.50	0.033	0.939	1.00	0.069	0.882	1.49	0.106	0.829
1	16	0.00390	0.707	0.25	0.055	0.806	0.50	0.121	0.652	0.89	0.290	0.437	1.21	0.512	0.304
4	16	0.00390	0.707	0.25	0.026	0.897	0.50	0.055	0.807	0.97	0.121	0.652	1.40	0.199	0.525
16	16	0.00390	0.707	0.25	0.013	0.948	0.50	0.026	0.898	0.99	0.055	0.807	1.47	0.086	0.725
1	16	2.33×10^{-10}	0.250	0.25	0.074	0.875	0.50	0.157	0.764	0.953	0.356	0.585	1.36	0.599	0.454
4	16	2.33×10^{-10}	0.250	0.25	0.036	0.940	0.50	0.074	0.879	0.99	0.157	0.761	1.46	0.251	0.666
16	16	2.33×10^{-10}	0.250	0.25	0.018	0.967	0.50	0.036	0.935	1.00	0.074	0.873	1.50	0.114	0.816
1	16	0.250	0.917	0.25	0.038	0.726	0.47	0.087	0.533	0.82	0.225	0.304	1.05	0.420	0.190
4	4	0.707	0.917	0.25	0.039	0.729	0.47	0.090	0.538	0.82	0.232	0.310	1.05	0.430	0.195
1	16	0.707	0.979	0.25	0.030	0.704	0.47	0.070	0.502	0.82	0.189	0.271	1.03	0.366	0.161

Table 5.1. Summary of suboptimum detector performance

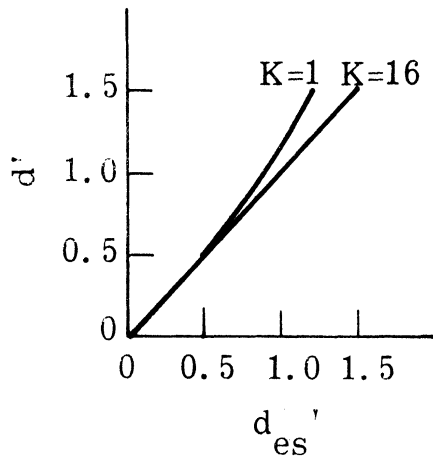
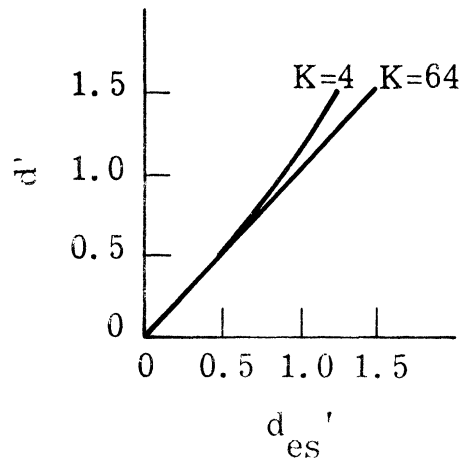
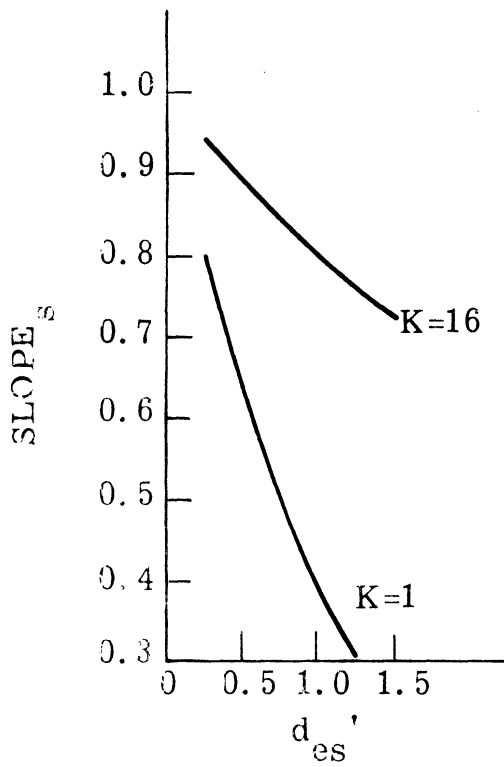
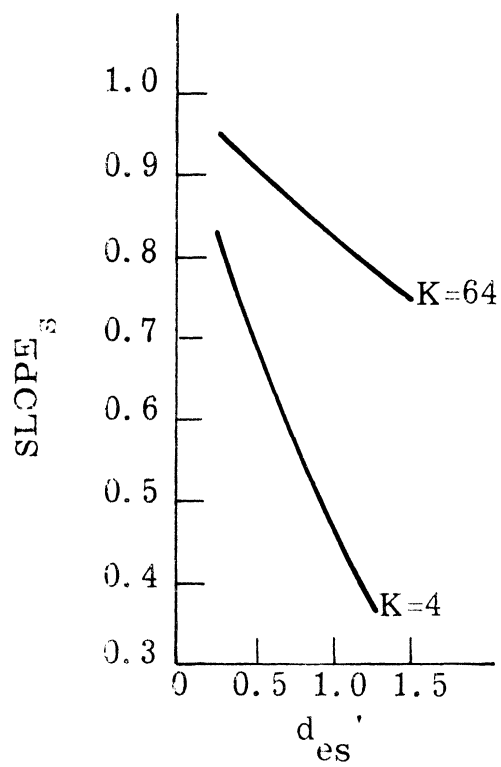
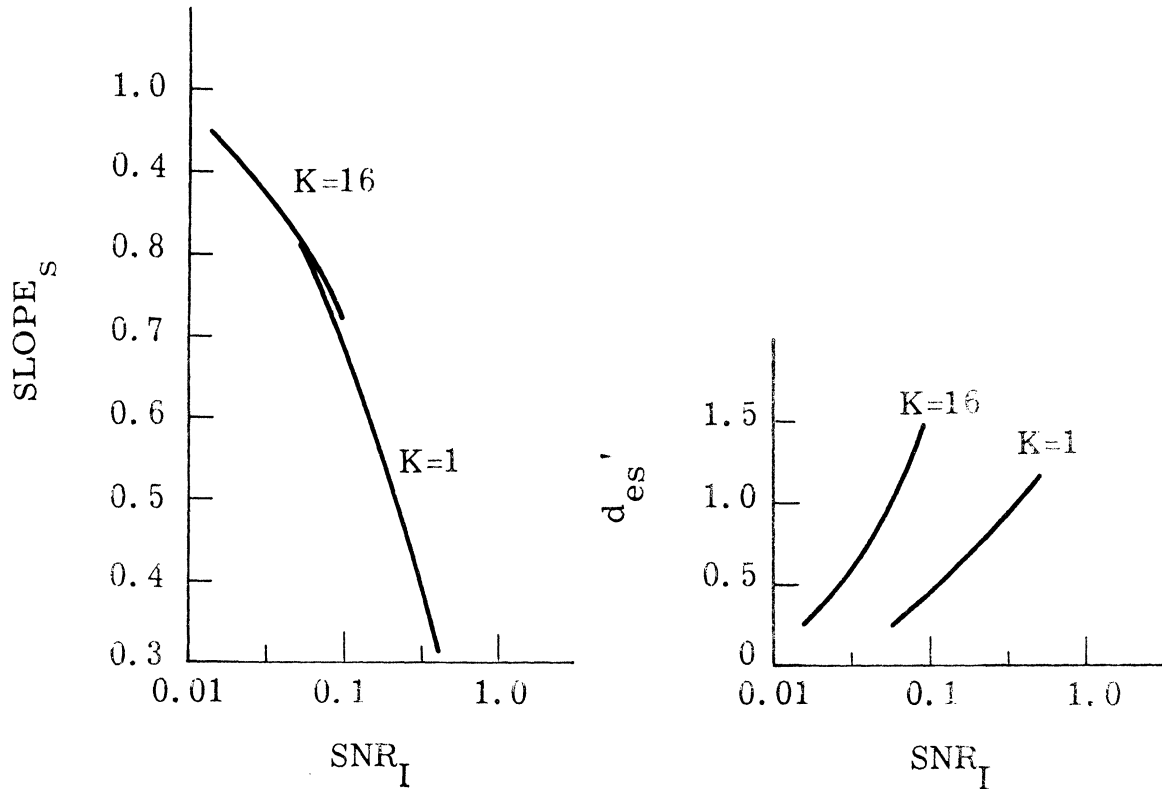
(a) d' vs. d'_{es} for $P = 16$ (b) d' vs. d'_{es} for $P = 4$ (c) $SLOPE_s$ vs. d'_{es} for $P = 16$ (d) $SLOPE_s$ vs. d'_{es} for $P = 4$

Fig. 5.3. Performance summary of the suboptimum detector as a function of d'_{es} for $\rho_s = 0.707$



(a) SLOPE_S vs. SNR_I for $\rho_S = 0.707$ (b) d'_{es} vs. SNR_I for $\rho_S = 0.707$

Fig. 5.4. Performance summary of the suboptimum detector as a function of SNR_I for P = 16

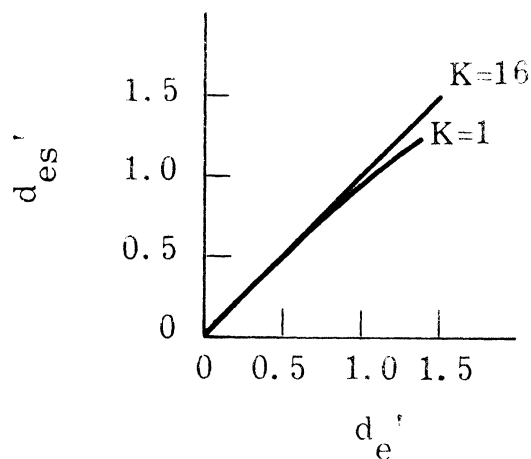


Fig. 5.5. Comparison of optimum and suboptimum detectability indexes for $\rho_S = 0.707$ and P = 16

It is finally seen that for the d' considered, the suboptimum performance, d_{es}' is sufficiently close to the optimum performance, d_e' , in the ROC evaluation region to say that the suboptimum detector performs almost as well as the optimum detector (Fig. 5.5). Consequently the optimum detector can be replaced by the suboptimum detector without any appreciable degradation in performance.

5.5 Summary

The suboptimum detector selected is the small SNR_I form of the optimum detector. The suboptimum performance is approximated in the ROC evaluation region by a binormal ROC on the basis of the Central Limit Theorem and the optimum ROC.

The suboptimum detector performs as well as the optimum detector. The slope of the suboptimum ROC is more binormal than the optimum ROC. The relationships between the detector parameters (K, P, ρ_s, ρ) is the same for the optimum and suboptimum detectors. However the suboptimum statistics are unbounded with increasing SNR_I under H_0 and H_1 while the optimum statistics are bounded under H_0 and unbounded under H_1 .

CHAPTER VI

CONCLUSIONS

6.1 Summary and Conclusions

The problem studied in this dissertation is the fixed time forced choice detection of Cyclo-Stationary (CS) processes in additive noise. CS processes are defined in Chapter I as those nonstationary random processes possessing autocorrelation matrices with a cyclic structure. CS processes normally arise from sampling continuous time CS processes. However other sampling schemes such as multiplexing samples from different stationary random processes or multiplexing samples from the sensors of an array observing a stationary random process also generate CS processes.

It is highly desirable to preserve the cyclic structure of the CS autocorrelation matrix in optimum detector expansions. Preserving the cyclic structure permits identification of the detector performance with specific properties of the autocorrelation matrix, as well as introducing a new interpretation for detector expansions.

The optimum detector becomes, when the cyclic structure of the CS autocorrelation matrix is preserved, a noise reduction filter followed by a signal enhancement filter followed by energy detection. The structure of the signal enhancement filter is clearly identifiable with the cyclic structure of the CS autocorrelation matrix.

The performance for the optimum detector is evaluated in Chapter IV for a WSCS Gauss-Markov random process. The performance evaluation is limited to a region called the ROC evaluation region where $0.01 \leq P_D \leq 0.99$ and $0.01 \leq P_{FA} \leq 0.9$. The optimum ROC behaves as a binormal ROC in the ROC evaluation region. This does not imply that the complete optimum ROC is binormal. The optimum ROC is normal for low SNR_I and deviates from that as SNR_I increases. Simultaneously the optimum performance is the same as the desired performance for low SNR_I and is less than the desired performance for large SNR_I where the desired performance is based on a normal ROC.

The optimum performance can be improved, less SNR_I for a given d' , by increasing the period-to-period correlation coefficient (ρ), the sample-to-sample correlation coefficient (ρ_s), the number of samples in a period (P), and the number of periods (K) observed, or any combination thereof.

The CS signal is usually specified in detection problems. Consequently ρ , ρ_s , and P are fixed, and the only way to improve the performance is to increase the observation time (K).

A suboptimum detector is derived in Chapter V. The suboptimum detector is presented in the belief that suboptimum detectors are generally easier to implement than optimum detectors. The suboptimum detector studied is the small SNR_I form of the optimum detector.

The statistics, mean and variance, of the optimum and sub-optimum decision variables, $\tilde{Z}[Y]$ and $\tilde{Z}_s[Y]$ respectively, under H_0 and H_1 are studied. The statistics of $\tilde{Z}[Y]$ under H_0 are bounded with increasing SNR_I but the statistics of $\tilde{Z}_s[Y]$ become unbounded under H_0 . The statistics of $\tilde{Z}[Y]$ and $\tilde{Z}_s[Y]$ under H_1 are unbounded with increasing SNR_I . Consequently the statistics of $\tilde{Z}_s[Y]$ are unbounded under H_0 and H_1 .

The performance of the suboptimum detector is approximated in the ROC evaluation region by a binormal ROC on the basis of the Central Limit Theorem and the optimum performance. The suboptimum performance, like the optimum performance, can only be improved by increasing ρ , ρ_s , P , K , or any combination thereof. The suboptimum performance is the same as the optimum performance for small SNR_I but is less for larger SNR_I . Simultaneously the slope of the suboptimum ROC is always less than the slope of the optimum ROC though for small SNR_I the suboptimum ROC is almost normal. The divergence in performance and slope between the optimum and suboptimum detectors is a result of the instability of the statistics of $\tilde{Z}_s[Y]$ with increasing SNR_I .

The suboptimum detector studied is an attractive alternative to the optimum detector. The suboptimum detector performs almost as well as the optimum detector and is easier to implement. However the instability of the statistics of $\tilde{Z}_s[Y]$ tempers the attractiveness of the suboptimum detector.

6.2 Contributions

The sufficient statistic for making optimum detections via the likelihood ratio for Gaussian signal in additive Gaussian noise is a quadratic form when the signal and noise autocorrelation matrices, R_S and R_N respectively, are known. A new interpretation for the quadratic form is presented which permits preserving the cyclic structure of the CS signal autocorrelation matrix. The quadratic form is

$$\tilde{Z}[Y] = Y^* \left[R_N^{-1} - [R_S + R_N]^{-1} \right] Y \quad (3.1)$$

The interpretation involves isolating R_S in two steps. The first step is applying the matrix identity

$$[R_S + R_N]^{-1} = R_N^{-1} - R_N^{-1} [R_S^{-1} + R_N^{-1}]^{-1} R_N^{-1}$$

to partially isolate R_S in $R_N^{-1} - [R_S + R_N]^{-1}$. The second step is to complete the isolation of R_S by simultaneously diagonalizing R_S and R_N . This is a new approach to simultaneous diagonalization because the usual approach is to simultaneously diagonalize the observation autocorrelation matrices under H_0 and H_1 , R_N and $R_S + R_N$ respectively.

Detecting a stationary random process with an array of sensors is equivalent to detecting a CS process. The carrier matrix comes from the correlations between the time samples at any

sensor. However the cyclic structure and the modulation matrix come from the spatial sampling introduced by the sensors. The array provides spatial information through the modulation matrix which is entirely different than classical beamforming. The modulation provides spatial information through the correlation properties between sensors while classical beamforming provides spatial information by introducing time delays in the sensor outputs to form beams.

6.3 Suggestions for Future Work

The whitening filter, W , is a nonrealizable filter in that future inputs are required for present outputs. The detector expansion would be more attractive if the whitening filter were realizable. If W is diagonal, the whitening filter is realizable; and if W is almost diagonal, the whitening filter is almost realizable. Under what conditions does the whitening filter become realizable or almost realizable?

The suboptimum detector studied is the small SNR_I form of the optimum detector. The suboptimum decision variable consists of the sum of the squares of independent Gaussian random variables. Since the whitening filter, W , does not add any energy to the output, the suboptimum detector would be more attractive if the whitening filter were absent because the simultaneous diagonalization problem need not be solved. However if the whitening filter is removed, the suboptimum decision variable becomes the sum of the squares of

dependent Gaussian random variables. The performance then becomes harder to evaluate. Studying the suboptimum detector without the whitening filter is an interesting problem for future work.

More work is needed to truly understand the relationship between the modulation matrix and spatial information for an array. How is the space around an array observed through the modulation matrix? Is the concept of steering an array meaningless when applied to a modulation matrix?

APPENDIX A
SIMULTANEOUS DIAGONALIZATION

A theorem on simultaneous diagonalization will be stated, and the proof (Refs. 11 and 27) paraphrased, and some properties resulting from the theorem will be derived. Before stating the theorem, some basic notation will be defined.

- a. A matrix, A , is Hermitian if

$$A = A^* \tag{A.1}$$

where $*$ denotes the complex conjugate (-) of the transpose (T).

- b. $\text{TR}[A]$ is the trace of the matrix A .
- c. The inner product of two column vectors, X and Y , is denoted as (X, Y) and is defined as

$$(X, Y) = X^*Y \tag{A.2}$$

- d. A Hermitian matrix, A , is positive definite if

$$(X, AY) > 0 \tag{A.3}$$

for all nonzero complex X and Y . Since A is Hermitian, it should be noted that

$$(X, AY) = (AX, Y) \tag{A.4}$$

Theorem: If A and B are Hermitian matrices, and if A is positive definite, there exists a complex matrix, U , of eigenvectors and a real diagonal matrix, Λ , of eigenvalues such that

$$U^*AU = I, \quad \text{and} \quad (\text{A.5})$$

$$U^*BU = \Lambda. \quad (\text{A.6})$$

Proof:

Solve the following eigenvalue problem where A and B are $N \times N$ dimensional matrices. Find the eigenvalues, λ_k , for which the equation

$$[B - \lambda_k A] X_k = 0 \quad (\text{A.7})$$

has a nontrivial solution. It follows that λ_k is an eigenvalue if and only if the following determinant is zero:

$$|B - \lambda_k A| = 0. \quad (\text{A.8})$$

Eq. A.8 is in general of the N th degree, and there will be N values for λ_k . For every distinct value of λ_k , there exists an eigenvector, X_k an N dimensional column vector, satisfying Eq. A.7. It is assumed that there are N distinct eigenvalues, λ_k , and corresponding eigenvectors, X_k .

Now from Eq. A.7

$$(X_k, BX_k) = \lambda_k (X_k, AX_k), \quad \text{and} \quad (\text{A. 9})$$

$$(BX_k, X_k) = \bar{\lambda}_k (AX_k, X_k). \quad (\text{A. 10})$$

Since A and B are Hermitian, Eq. A.4

$$(X_k, BX_k) = (BX_k, X_k), \quad \text{and} \quad (\text{A. 11})$$

$$(X_k, AX_k) = (AX_k, X_k). \quad (\text{A. 12})$$

Therefore by Eqs. A.9 - A.12,

$$\lambda_k = \bar{\lambda}_k, \quad (\text{A. 13})$$

and the eigenvalues are real.

Since A and B are Hermitian, and the eigenvalues are real, Eqs. A.4, A.7, and A.13,

$$\begin{aligned} 0 &= (X_k, BX_m) - (BX_k, X_m) \\ &= \lambda_m (X_k, AX_m) - \lambda_k (AX_k, X_m) \\ &= (\lambda_m - \lambda_k) (X_k, AX_m) \end{aligned} \quad (\text{A. 14})$$

It then follows that for $\lambda_m \neq \lambda_k$, the corresponding eigenvectors, X_m and X_k , are orthogonal with respect to A.

$$(X_k, AX_m) = 0 \quad \text{for } k \neq m. \quad (\text{A. 15})$$

Since A is positive definite, Eq. A.4,

$$(X_k, AX_k) > 0. \quad (\text{A.16})$$

It then follows that the X_k can be normalized so that

$$(X_k, AX_m) = \delta_{km}, \quad \text{and} \quad (\text{A.17})$$

$$(X_k, BX_m) = (X_k, \lambda_m AX_m) = \lambda_m \delta_{km} \quad (\text{A.18})$$

where δ_{km} is the Kronecker delta

$$\delta_{km} = \begin{cases} 1, & k = m \\ 0, & k \neq m \end{cases} \quad (\text{A.19})$$

Now let U be the matrix whose columns are the normalized eigenvectors X_k , and Λ be the real diagonal matrix whose diagonal elements are the eigenvalues λ_k . It follows that the theorem is proved, Eqs. A.17 and A.18.

Corollary 1 (C1):

If B is positive definite

$$\text{TR}[\Lambda^{-1}] = \text{TR}[AB^{-1}]. \quad (\text{A.20})$$

Proof:

Since A is nonsingular, U has an inverse. Let

$$U^{-1} = Q . \quad (\text{A.21})$$

Then

$$B = Q^* \Lambda Q ; \quad (\text{A.22})$$

$$\begin{aligned} B^{-1} &= Q^{-1} \Lambda^{-1} Q^{*-1} \\ &= U \Lambda^{-1} U^* , \text{ and} \end{aligned} \quad (\text{A.23})$$

$$A = Q^* Q . \quad (\text{A.24})$$

Then

$$\begin{aligned} AB^{-1} &= Q^* Q Q^{-1} \Lambda^{-1} Q^{*-1} \\ &= Q^* \Lambda^{-1} U^* . \end{aligned} \quad (\text{A.25})$$

AB^{-1} has the elements

$$AB^{-1} = \sum_{p=1}^N \bar{q}_{kp} \lambda_p^{-1} \bar{u}_{pm} \quad \text{for } k, m = 1, 2, \dots, N \quad (\text{A.26})$$

where q_{kp} and u_{pm} are the elements of Q and U respectively.

$$\begin{aligned} \text{TR}[AB^{-1}] &= \sum_{k=1}^N \sum_{p=1}^N \bar{q}_{kp} \lambda_p^{-1} \bar{u}_{pk} \\ &= \sum_{p=1}^N \lambda_p^{-1} \sum_{k=1}^N \bar{q}_{kp} \bar{u}_{pk} . \end{aligned} \quad (\text{A.27})$$

Now for any $p = 1, 2, \dots, N$, Eq. A.21 implies

$$\sum_{k=1}^N q_{kp} \bar{u}_{pk} = 1 . \quad (\text{A.28})$$

Therefore Eq. A.20 holds.

Corollary 2 (C2): There exists a unitary matrix W and a lower triangular matrix L such that

$$A = L^*L , \quad \text{and} \quad (\text{A.29})$$

$$WL = Q . \quad (\text{A.30})$$

The existence of the lower triangular matrix L is proved by the Guilleman (Ref. 12). The unitary matrix W has the following property:

$$W^*W = WW^* = I . \quad (\text{A.31})$$

Since A has an inverse so does L . From (A.30)

$$W = QL^{-1} . \quad (\text{A.32})$$

Multiply the right sides of Eq. A.32 by W^* .

$$\begin{aligned} WW^* &= QL^{-1}L^{-1*}Q^* \\ &= QA^{-1}Q^* \\ &= I \end{aligned} \quad (\text{A.33})$$

by Eq. A.29. Multiply the left sides of Eq. A.32 by W^*

$$\begin{aligned}W^*W &= L^{-1*} Q^* Q L^{-1} \\ &= L^{-1*} A L^{-1} \\ &= I\end{aligned}\tag{A.34}$$

by Eq. A.29.

Q.E.D.

APPENDIX B
REALIZABILITY

Realizability is a nebulous concept when applied to digital computers. Digital computers can easily delay inputs by using storage. However in many cases the storage is limited, and the concept of providing increasingly large delay breaks down. The concept of realizability really implies that future events do not affect the present response.

Let the matrix H be a filter with input X and output Y . Let H , Y , and X have the elements h_{lk} , y_l , x_k respectively. Then

$$y_l = \sum_{k=1}^N h_{lk} x_k . \quad (B.1)$$

H is said to be realizable if

$$y_l = \sum_{k=1}^l h_{lk} x_k . \quad (B.2)$$

Therefore from Eq. B.2, H is a realizable matrix if H is a lower triangular matrix.

APPENDIX C

PARAMETERS OF THE BINORMAL ROC

The detectability index, d_e' , and SLOPE for a binormal ROC will be derived in terms of the first two moments of the decision variable, Z , under H_0 and H_1 . Let

$$Z \sim \begin{cases} N(m_0, \sigma_0^2), & H_0 \\ N(m_1, \sigma_1^2), & H_1 \end{cases} .$$

It then follows that

$$P_D = \int_{\alpha}^{\infty} \frac{1}{\sqrt{2\pi} \sigma_1} e^{-\frac{(Z - m_1)^2}{2\sigma_1^2}} dz \quad (C.1)$$

and

$$P_{FA} = \int_{\alpha}^{\infty} \frac{1}{\sqrt{2\pi} \sigma_0} e^{-\frac{(Z - m_0)^2}{2\sigma_0^2}} dz . \quad (C.2)$$

Equivalently

$$P_D = \Phi(X_1) \quad (C.3)$$

and

$$P_{FA} = \Phi(X_0) \quad (C.4)$$

where

$$1. \quad \Phi(\alpha) = \frac{1}{\sqrt{2\pi}} \int_{-\infty}^{\alpha} e^{-t^2/2} dt .$$

$$2. \quad X_1 = - \frac{\alpha - m_1}{\sigma_1} .$$

$$3. \quad X_0 = - \frac{\alpha - m_0}{\sigma_0} .$$

Since the binormal ROC is a straight line when plotted on normal-normal graph paper, it is of interest to solve for SLOPE and β in the equation

$$X_1 = \text{SLOPE } X_0 + \beta \quad (C.5)$$

The two ROC points used to solve for β and SLOPE in Eq. C.5 are the $P_D = 0.5$ and $P_{FA} = 0.5$ points. When $P_D = 0.5$,

$$X_1' = 0$$

and (C.6)

$$X_0' = - \frac{m_1 - m_0}{\sigma_0} .$$

When $P_{FA} = 0.5$,

$$X_1'' = \frac{m_1 - m_0}{\sigma_1}$$

and

$$X_0'' = 0 . \quad (C.7)$$

Substitute Eqs. C.6 and C.7 into Eq. C.5.

$$X_1 = \frac{\sigma_0}{\sigma_1} X_0 + \frac{m_1 - m_0}{\sigma_1} \quad (C.8)$$

The detectability index d_0' at a given P_D and P_{FA} for a normal ROC is the intersection of that straight line of unity slope passing through the point (P_D, P_{FA}) and the negative diagonal. It is a measure of the distance between P_D and P_{FA} . That is

$$P_D = \Phi|X_0 + d_0'| ,$$

$$P_{FA} = \Phi|X_0| ,$$

and

$$d_0' = X_1 - X_0 . \quad (C.9)$$

Substitute Eq. C.8 into Eq. C.9

$$d_0' = \frac{\sigma_0 - \sigma_1}{\sigma_1} X_0 + \frac{m_1 - m_0}{\sigma_1} . \quad (C.10)$$

d_e' is the detectability index at the intersection of the binormal ROC and the negative diagonal.

$$\frac{d_e'}{2} = X_1 = -X_0 . \quad (\text{C.11})$$

Substitute Eq. C.11 into Eq. C.10. It follows that

$$d_e' = \frac{2(m_1 - m_0)}{\sigma_1 + \sigma_0} . \quad (\text{C.12})$$

It also follows from Eqs. C.5 and C.8 that

$$\text{SLOPE} = \sigma_0 / \sigma_1 . \quad (\text{C.13})$$

APPENDIX D

EIGENVALUES AND INPUT SIGNAL-TO-NOISE RATIOS

Let R_S and R_N be the signal and noise correlation matrices respectively. Simultaneously diagonalize R_S and R_N as (Appendix A)

$$R_S = Q^* Q \quad (D.1)$$

and

$$R_N = Q^* \Lambda Q \quad (D.2)$$

where

1. $Q = \{q_{nm}\}$, $n, m = 1, 2, \dots, N$.
2. The diagonal elements of Λ are the eigenvalues

$$\lambda_n, \quad n = 1, 2, \dots, N.$$

The input signal-to-noise ratio, SNR_I , is

$$\begin{aligned} SNR_I &= \frac{\frac{1}{KP} \text{TR}[R_S]}{\frac{1}{KP} \text{TR}[R_N]} \\ &= \frac{\text{TR}[R_S]}{\text{TR}[R_N]} \end{aligned} \quad (D.3)$$

where $\text{TR}[]$ is the trace of the matrix in the brackets.

It then follows from Eqs. D.1 and D.2 that

$$\text{TR}[\mathbf{R}_S] = \sum_{n, m=1}^N \bar{q}_{nm} q_{mn} \quad (\text{D.4})$$

and

$$\text{TR}[\mathbf{R}_N] = \sum_{n, m=1}^N \bar{q}_{nm} \lambda_n q_{mn} \quad (\text{D.5})$$

where $\bar{}$ denotes complex conjugate. Substitute Eqs. D.4 and D.5 into D.3.

$$\text{SNR}_I = \frac{\sum_{n, m=1}^N \bar{q}_{nm} q_{mn}}{\sum_{n, m=1}^N \bar{q}_{nm} \lambda_n q_{mn}} \quad (\text{D.6})$$

The size of the eigenvector noise-to-signal ratio, λ_n , is inversely proportional to the size of SNR_I . Consequently the size of the eigenvector signal-to-noise ratio, λ_n^{-1} , is directly proportional to the size of SNR_I .

APPENDIX E

EXAMPLE OF FACTORIZING THE AUTOCORRELATION

MATRIX OF A WSCS PROCESS

Consider sampling the WSCS process

$$s(t) = x(t) \cos \omega_0 t$$

where $x(t)$ is a real zero-mean Wide Sense Stationary Gauss Markov Process with correlation function

$$R_x(\tau) = R_x(0) e^{-\alpha |\tau|} .$$

The frequency, ω_0 , is assumed known. There are exactly P samples in a period. Let the sampling interval, T_s , be

$$T_s = \frac{1}{Pf_0} .$$

Then

$$\begin{aligned} s \left[(n-1) T_s \right] &= x \left[\frac{(n-1)}{Pf_0} \right] \cos 2\pi f_0 \left[\frac{(n-1)}{Pf_0} \right] \\ &= x \left[\frac{(n-1)}{Pf_0} \right] \cos \frac{2\pi}{P} \frac{(n-1)}{P} \quad \text{for } n = 1, 2, 3, \dots \end{aligned}$$

Consider the correlation between $s[(n-1)T_s]$ and $s[(m-1)T_s]$.

$$\begin{aligned} r_s(n, m) &= E \left\{ s[(n-1)T_s] s[(m-1)T_s] \right\} \\ &= \frac{R_x \left[\frac{m-n}{Pf_0} \right]}{2} \left[\cos \frac{2\pi(m+n-2)}{P} + \cos \frac{2\pi(m-n)}{P} \right] \end{aligned}$$

ρ_s is the normalized correlation coefficient between adjacent samples.

$$\rho_s = \frac{R_x \left(\frac{1}{Pf_0} \right)}{R_x(0)} .$$

Then

$$r_s(n, m) = \frac{R_x(0) \rho_s^{|m-n|}}{2} \left[\cos \frac{2\pi(m+n-2)}{P} + \cos \frac{2\pi(m-n)}{P} \right] .$$

Assume that $P = 2$ and $K = 3$, i. e. , there are three periods in the observation and there are two samples in a period. Also assume $R_x(0) = 1$. The autocorrelation matrix is

$$R_S = \{r_s(n, m)\} \quad \text{for } n, m = 1, 2, 3, 4, 5, 6 .$$

For this case, R_S has the structure of the autocorrelation matrix of a Wide Sense Stationary random process.

$$R_S = \left[\begin{array}{cc|cc|cc} 1 & -\rho_S & \rho_S^2 & -\rho_S^3 & \rho_S^4 & -\rho_S^5 \\ -\rho_S & 1 & -\rho_S & \rho_S^2 & -\rho_S^3 & \rho_S^4 \\ \hline \rho_S^2 & -\rho_S & 1 & -\rho_S & \rho_S^2 & -\rho_S^3 \\ -\rho_S^3 & \rho_S & -\rho_S & 1 & -\rho_S & \rho_S^2 \\ \hline \rho_S^4 & -\rho_S^3 & \rho_S^2 & -\rho_S & 1 & -\rho_S \\ -\rho_S^5 & \rho_S^4 & -\rho_S^3 & \rho_S^2 & -\rho_S & 1 \end{array} \right]$$

From this we get the submatrices

$$A = \begin{bmatrix} 1 & -\rho_S \\ -\rho_S & 1 \end{bmatrix}, \quad A_{12} = \begin{bmatrix} \rho_S^2 & -\rho_S^3 \\ -\rho_S & \rho_S^2 \end{bmatrix} = A_{23},$$

$$A_{13} = \begin{bmatrix} \rho_S^4 & -\rho_S^5 \\ -\rho_S^3 & \rho_S^4 \end{bmatrix}, \quad A_{21} = \begin{bmatrix} \rho_S^2 & -\rho_S \\ -\rho_S^3 & \rho_S^2 \end{bmatrix} = A_{32},$$

$$A_{31} = \begin{bmatrix} \rho_S^4 & -\rho_S^3 \\ -\rho_S^5 & \rho_S^4 \end{bmatrix}.$$

In this case it is evident that

$$A_{13} = \rho_S^2 A_{12},$$

and

$$A_{31} = \rho_S^2 A_{21}.$$

$$R_S = \begin{bmatrix} A & A_{12} & \rho_S^2 A_{12} \\ A_{21} & A & A_{12} \\ \rho_S^2 A_{21} & A_{21} & A \end{bmatrix} .$$

The modulation matrix, M, becomes

$$M = \begin{bmatrix} \sqrt{1-\rho_S^2} & 0 \\ -\rho_S & 1 \end{bmatrix} \text{ and}$$

$$M^{-1} = \frac{1}{\sqrt{1-\rho_S^2}} \begin{bmatrix} 1 & 0 \\ \rho_S & \sqrt{1-\rho_S^2} \end{bmatrix}$$

where $R_S = M^* M$.

The T_{nm} are defined as

$$T_{nm} = M^{-1*} A_{nm} M^{-1} .$$

Then

$$\begin{aligned} T_{12} &= \frac{1}{\sqrt{1-\rho_S^2}} \begin{bmatrix} 1 & \rho_S \\ 0 & \sqrt{1-\rho_S^2} \end{bmatrix} \begin{bmatrix} \rho_S^2 & -\rho_S^3 \\ -\rho_S & \rho_S^2 \end{bmatrix} \begin{bmatrix} 1 & 0 \\ \rho_S & \sqrt{1-\rho_S^2} \end{bmatrix} \frac{1}{\sqrt{1-\rho_S^2}} \\ &= \begin{bmatrix} 0 & 0 \\ -\rho_S \sqrt{1-\rho_S^2} & \rho_S^2 \end{bmatrix} . \end{aligned}$$

$$\begin{aligned}
T_{13} &= M^{-1*} \rho_S^2 A_{12} M^{-1} = \rho_S^2 T_{12} \\
&= \begin{bmatrix} 0 & 0 \\ -\rho_S^3 \sqrt{1-\rho_S^2} & \rho_S^4 \end{bmatrix} .
\end{aligned}$$

Similarly

$$T_{21} = \begin{bmatrix} 0 & -\rho_S \sqrt{1-\rho_S^2} \\ 0 & \rho_S^2 \end{bmatrix}$$

and

$$T_{31} = \rho_S^2 T_{21} = \begin{bmatrix} 0 & -\rho_S^3 \sqrt{1-\rho_S^2} \\ 0 & \rho_S^4 \end{bmatrix} .$$

Consequently

$$\begin{aligned}
M_3 &= \begin{bmatrix} M & 0 & 0 \\ 0 & M & 0 \\ 0 & 0 & M \end{bmatrix} \\
&= \begin{bmatrix} \sqrt{1-\rho_S^2} & 0 & 0 & 0 & 0 & 0 \\ -\rho_S & 1 & 0 & 0 & 0 & 0 \\ 0 & 0 & \sqrt{1-\rho_S^2} & 0 & 0 & 0 \\ 0 & 0 & -\rho_S & 1 & 0 & 0 \\ 0 & 0 & 0 & 0 & \sqrt{1-\rho_S^2} & 0 \\ 0 & 0 & 0 & 0 & -\rho_S & 1 \end{bmatrix}
\end{aligned}$$

and

$$T = \begin{bmatrix} T_{11} & T_{12} & T_{13} \\ T_{21} & T_{11} & T_{12} \\ T_{31} & T_{21} & T_{11} \end{bmatrix} .$$

$$T = \left[\begin{array}{cc|cc|cc} 1 & 0 & 0 & 0 & 0 & 0 \\ 0 & 1 & -\rho_S \sqrt{1-\rho_S^2} & \rho_S^2 & -\rho_S^3 \sqrt{1-\rho_S^2} & \rho_S^4 \\ \hline 0 & -\rho_S \sqrt{1-\rho_S^2} & 1 & 0 & 0 & 0 \\ 0 & \rho_S^2 & 0 & 1 & -\rho_S \sqrt{1-\rho_S^2} & \rho_S^2 \\ \hline 0 & -\rho_S^3 \sqrt{1-\rho_S^2} & 0 & -\rho_S \sqrt{1-\rho_S^2} & 1 & 0 \\ 0 & \rho_S^4 & 0 & \rho_S^2 & 0 & 1 \end{array} \right] .$$

From $T = C^* C$, we get the carrier matrix.

$$C = \left[\begin{array}{cc|cc|cc} 1 & 0 & 0 & 0 & 0 & 0 \\ 0 & \sqrt{1-\rho_S^2} & 0 & 0 & 0 & 0 \\ \hline 0 & -\rho_S \sqrt{1-\rho_S^2} & 1 & 0 & 0 & 0 \\ 0 & \rho_S^2 \sqrt{1-\rho_S^2} & 0 & \sqrt{1-\rho_S^2} & 0 & 0 \\ \hline 0 & -\rho_S^3 \sqrt{1-\rho_S^2} & 0 & -\rho_S \sqrt{1-\rho_S^2} & 1 & 0 \\ 0 & \rho_S^4 & 0 & \rho_S^2 & 0 & 1 \end{array} \right] = \begin{bmatrix} C_{11} & C_{12} & C_{13} \\ C_{21} & C_{22} & C_{23} \\ C_{31} & C_{32} & C_{33} \end{bmatrix} .$$

Now

$$C_{11} = \begin{bmatrix} 1 & 0 \\ 0 & \sqrt{1-\rho_s^2} \end{bmatrix},$$

$$C_{12} = C_{13} = C_{23} = 0,$$

$$C_{21} = \begin{bmatrix} 0 & -\rho_s \sqrt{1-\rho_s^2} \\ 0 & \rho_s^2 \sqrt{1-\rho_s^2} \end{bmatrix},$$

$$C_{22} = C_{11},$$

$$C_{31} = T_{31}, \quad C_{32} = T_{32}, \quad C_{33} = T_{33}.$$

REFERENCES

1. Bello, P., "Some Results on the Problem of Discriminating between Two Gaussian Process," IRE Trans. Information Theory, 1961, Vol. IT-7, No. 4, pp. 224-233.
2. Birdsall, T. G., The Theory of Signal Detectability: ROC Curves and Their Character, Ph.D. dissertation at the University of Michigan, Ann Arbor, Michigan, 1966.
3. Bryn, F., "Optimum Signal Processing of Three-Dimensional Arrays Operating on Gaussian Signals and Noise," JASA, 1962, Vol. 34, No. 3, pp. 289-297.
4. Cooley, J. W., Lewis, P. A. W., and Welch, P. D., "Application of the Fast Fourier Transform to Computation of Fourier Integrals, Fourier Series, and Convolution Integrals," IEEE Trans. Audio and Electroacoustics, 1967, Vol. AU-15, No. 2, pp. 79-84.
5. Cooley, J. W., Lewis, P. A. W., and Welch, P. D., "The Fast Fourier Transform Algorithm: Programming Considerations in the Calculation of Sine, Cosine, and Laplace Transforms," J. Sound Vib., 1970, Vol. 12, No. 3, pp. 315-337.
6. Chang, J. H. and Tuteur, F. B., "A New Class of Adaptive Processors," JASA, 1971, Vol. 49, No. 3, pp. 639-649.
7. Cramér, H., Mathematical Methods of Statistics, Princeton, Princeton University Press, 1951, Chap. 24.
8. Davis, R. C., "The Detectability of Random Signals in the Presence of Noise," IRE Trans. Information Theory, 1957, Vol. IT-3, pp. 52-62.
9. Deutch, R., "Detection of Modulated Noise-Like Signals," Trans. IRE Professional Group on Information Theory, 1954, Vol. PGIT-3, pp. 106-122.
10. Doob, J. L., Stochastic Processes, New York, John Wiley and Sons, Inc., 1953, Chap. 10, Art. 3.
11. Friedman, B., Principles and Techniques of Applied Mathematics, New York, John Wiley and Sons, Inc., 1956, pp. 107-109.

REFERENCES (Cont.)

12. Guillemin, E. A., The Mathematics of Circuit Analysis, New York, John Wiley and Sons, Inc., 1944, Chap. 4, Art. 9.
13. Hariharan, P. R., "Detection of Modulated Gaussian Signals in Noise," IEEE Trans. Commun. Technol., 1972, Vol. COM 20, No. 1, pp. 28-37.
14. Hurd, H. L., An Investigation of Periodically Correlated Stochastic Processes, Ph.D. dissertation at Duke University, Durham, N. C., 1970.
15. Johnson, N. L., and Katz, S., Distributions in Statistics, New York, Houghton Mifflin, 1969.
16. Kailath, T., "A General Likelihood-Ratio Formula for Random Signals in Noise," IEEE Trans. Information Theory, 1969, Vol. IT-5, No. 3, pp. 350-361.
17. Kailath, T., "Correlation Detection of Signals Perturbed by a Random Channel," IRE Trans. Information Theory, 1960, Vol. IT-6, No. 3, pp. 361-366.
18. Kincaid, T. G., The Adaptive Detection and Estimation of Nearby Periodic Signals, General Electric Co., Research and Development Center, Schenectady, N. Y., Technical Report S-69-1139, 1969.
19. Middleton, D., "On the Detection of Stochastic Signals in Additive Normal Noise, I," IRE Trans. Information Theory, 1957, Vol. IT-8, No. 3, pp. 86-121.
20. Middleton, D., "On the Detection of Stochastic Signals in Additive Normal Noise, II," IRE Trans. Information Theory, 1960, Vol. IT-6, pp. 349-360.
21. Middleton, D. and Groginsky, H. L., "Detection of Random Acoustic Signals by Receivers with Distributed Elements: Optimum Receiver Structures for Normal Signal and Noise Fields," JASA, 1965, Vol. 38, No. 5, pp. 727-737.

REFERENCES (Cont.)

22. Parzen, E. and Shirer, N. , "Analysis of a General System for the Detection of Amplitude-Modulated Noise," JASA, 1965, Vol. 35, pp. 278-288.
23. Peterson, W. W. , Birdsall, T. G. , and Fox, W. C. , "The Theory of Signal Detectability," Trans. IRE Professional Group on Information Theory, 1954, PGIT-4, pp. 171-211. Also Peterson, W. W. , Birdsall, T. G. , The Theory of Signal Detectability, Electronic Defense Group Technical Report No. 13, Electronic Defense Group, The University of Michigan, Ann Arbor, Michigan, 1953.
24. Ristenbatt, M. P. , Investigations of Narrowband Waveforms Generated by Clocked Pulses, Cooley Electronics Laboratory Technical Report No. 112, Cooley Electronics Laboratory, The University of Michigan, Ann Arbor, Michigan, 1960.
25. Schwartz, S. C. , "A Series Technique for the Optimum Detection of Stochastic Signals in Noise," IEEE Trans. Information Theory, 1969, Vol. IT-15, No. 3, pp. 362-370.
26. Slepian, D. , "Some Comments on the Detection of Gaussian Signals in Gaussian Noise," IRE Trans. Information Theory, 1958, Vol. IT-4, pp. 65-68.
27. Stoll, R. R. , Linear Algebra and Matrix Theory, New York, McGraw-Hill Book Company, Inc. , 1952, pp. 259-260.
28. Thomas, J. B. and Williams, T. R. , "On the Detection of Signals in Nonstationary Noise by Product Arrays," JASA, 1959, Vol. 31, No. 4, pp. 453-462.
29. Usher, Jr. , T. , "Signal Detection by Arrays in Noise Fields with Local Variations," JASA, 1964, Vol. 36, No. 8, pp. 1444-1449.
30. Usher, Jr. , T. , "Signal Detection by Arrays with Arbitrary Processes and Detectors," JASA, 1966, Vol. 39, No. 1, pp. 79-86.
31. Van Trees, H. L. , Detection, Estimation, and Modulation Theory, Part III, New York, John Wiley and Sons, Inc. , 1971.

DISTRIBUTION LIST

	<u>No. of Copies</u>
Office of Naval Research (Code 468)	1
(Code 102-OS)	1
(Code 480)	1
Navy Department Washington, D. C. 20360	
Director, Naval Research Laboratory Technical Information Division Washington, D. C. 20390	6
Director Office of Naval Research Branch Office 1030 East Green Street Pasadena, California 91101	1
Dr. Christopher V. Kimball 8441 S.W. 142 Street Miami, Florida 33149	1
Director Office of Naval Research Branch Office 495 Summer Street Boston, Massachusetts 02210	1
Office of Naval Research New York Area Office 207 West 24th Street New York, New York 10011	1
Director Office of Naval Research Branch Office 536 S. Clark Street Chicago, Illinois 60605	1
Director Naval Research Laboratory Attn: Library, Code 2029 (ONRL) Washington, D. C. 20390	8

DISTRIBUTION LIST (Cont.)

	<u>No. of Copies</u>
Commander Naval Ordnance Laboratory Acoustics Division White Oak, Silver Spring, Maryland 20907 Attn: Dr. Zaka Slawsky	1
Commanding Officer Naval Ship Research & Development Center Annapolis, Maryland 21401	1
Commander Naval Undersea Research & Development Center San Diego, California 92132 Attn: Dr. Dan Andrews Mr. Henry Aurand	2
Chief Scientist Navy Underwater Sound Reference Division P. O. Box 8337 Orlando, Florida 32800	1
Commanding Officer and Director Navy Underwater Systems Center Fort Trumbull New London, Connecticut 06321	1
Commander Naval Air Development Center Johnsville, Warminster, Pennsylvania 18974	1
Commanding Officer and Director Naval Ship Research and Development Center Washington, D. C. 20007	1
Superintendent Naval Postgraduate School Monterey, California 93940	1
Commanding Officer & Director Naval Ship Research & Development Center* Panama City, Florida 32402	1

* Formerly Mine Defense Lab.

DISTRIBUTION LIST (Cont.)

	<u>No. of Copies</u>
Naval Underwater Weapons Research & Engineering Station Newport, Rhode Island 02840	1
Superintendent Naval Academy Annapolis, Maryland 21401	1
Scientific and Technical Information Center 4301 Suitland Road Washington, D. C. 20390 Attn: Dr. T. Williams Mr. E. Bissett	2
Commander Naval Ordnance Systems Command Code ORD-03C Navy Department Washington, D. C. 20360	1
Commander Naval Ship Systems Command Code SHIPS 037 Navy Department Washington, D. C. 20360	1
Commander Naval Ship Systems Command Code SHIPS 00V1 Washington, D. C. 20360 Attn: CDR Bruce Gilchrist Mr. Carey D. Smith	2
Commander Naval Undersea Research & Development Center 3202 E. Foothill Boulevard Pasadena, California 91107	1
Commanding Officer Fleet Numerical Weather Facility Monterey, California 93940	1

DISTRIBUTION LIST (Cont.)

	<u>No. of Copies</u>
Defense Documentation Center Cameron Station Alexandria, Virginia 22314	5
Dr. James Probus Office of the Assistant Secretary of the Navy (R&D) Room 4E741, The Pentagon Washington, D. C. 20350	1
Mr. Allan D. Simon Office of the Secretary of Defense DDR&E Room 3E1040, The Pentagon Washington, D. C. 20301	1
Capt. J. Kelly Naval Electronics Systems Command Code EPO-3 Washington, D. C. 20360	1
Chief of Naval Operations Room 5B718, The Pentagon Washington, D. C. 20350 Attn: Mr. Benjamin Rosenberg	1
Chief of Naval Operations Rm 4C559, The Pentagon Washington, D. C. 20350 Attn: CDR J. M. Van Metre	1
Chief of Naval Operations 801 No. Randolph St. Arlington, Virginia 22203	1
Dr. Melvin J. Jacobson Rensselaer Polytechnic Institute Troy, New York 12181	1
Dr. Charles Stutt General Electric Co. P. O. Box 1088 Schenectady, New York 12301	1

DISTRIBUTION LIST (Cont.)

	<u>No. of Copies</u>
Dr. Alan Winder EDO Corporation College Point, New York 11356	1
Dr. T. G. Birdsall Cooley Electronics Laboratory The University of Michigan Ann Arbor, Michigan 48105	1
Mr. Morton Kronengold Director, Institute for Acoustical Research 615 S.W. 2nd Avenue Miami, Florida 33130	1
Mr. Robert Cunningham Bendix Corporation 11600 Sherman Way North Hollywood, California 91606	1
Dr. H. S. Hayre University of Houston Cullen Boulevard Houston, Texas 77004	1
Mr. Ray Veenkant Texas Instruments, Inc. North Central Expressway Dalla, Texas 75222 Mail Station 208	1
Dr. Stephen Wolff John Hopkins University Baltimore, Maryland 21218	1
Dr. Bruce P. Bogert Bell Telephone Laboratories Whippany Road Whippany, New Jersey 07981	1
Dr. Albert Nuttall Navy Underwater Systems Center Fort Trumbull New London, Connecticut 06320	1

DISTRIBUTION LIST (Cont.)

	<u>No. of Copies</u>
Dr. Philip Stocklin Raytheon Company P. O. Box 360 Newport, Rhode Island 02841	1
Dr. H. W. Marsh Navy Underwater Systems Center Fort Trumbull New London, Connecticut 06320	1
Dr. David Middleton 35 Concord Ave., Apt. #1 Cambridge, Massachusetts 02138	1
Mr. Richard Vesper Perkin-Elmer Corporation Electro-Optical Division Norwalk, Connecticut 06852	1
Dr. Donald W. Tufts University of Rhode Island Kingston, Rhode Island 02881	1
Dr. Loren W. Nolte Dept. of Electrical Engineering Duke University Durham, North Carolina 27706	1
Dr. Thomas W. Ellis Texas Instruments, Inc. 13500 North Central Expressway Dallas, Texas 75231	1
Mr. Robert Swarts Honeywell, Inc. Marine Systems Center 5303 Shilshole Ave., N.W. Seattle, Washington, 98107	1
Mr. Charles Loda Institute for Defense Analyses 400 Army-Navy Drive Arlington, Virginia 22202	1

DISTRIBUTION LIST (Cont.)

	<u>No. of Copies</u>
Mr. Beaumont Buck General Motors Corporation Defense Research Division 6767 Holister Ave. Goleta, California 93017	1
Dr. M. Weinstein Underwater Systems, Inc. 8121 Georgia Avenue Silver Spring, Maryland 20910	1
Dr. Harold Saxton 1601 Research Blvd. TRACOR, Inc. Rockville, Maryland 20850	1
Dr. Thomas G. Kincaid General Electric Company P. O. Box 1088 Schenectady, New York 12305	1
Applied Research Laboratories The University of Texas at Austin Austin, Texas 78712 Attn: Dr. Loyd Hampton Dr. Charles Wood	3
Dr. Paul McElroy Woods Hole Oceanographic Institution Woods Hole, Massachusetts 02543	1
Dr. John Bouyoucos Hydroacoustics, Inc. P. O. Box 3818 Rochester, New York 14610	1
Dr. Joseph Lapointe Systems Control, Inc. 260 Sheridan Avenue Palo Alto, Calif. 94306	1
Cooley Electronics Laboratory University of Michigan Ann Arbor, Michigan 48105	25

DOCUMENT CONTROL DATA - R & D

(Security classification of title, body of abstract and indexing annotation must be entered when the overall report is classified)

1. ORIGINATING ACTIVITY (Corporate author)		2a. REPORT SECURITY CLASSIFICATION	
Cooley Electronics Laboratory The University of Michigan Ann Arbor, Michigan 48105		Unclassified	
3. REPORT TITLE		2b. GROUP	
THE THEORY OF SIGNAL DETECTABILITY: CYCLO-STATIONARY PROCESSES IN ADDITIVE NOISE			
4. DESCRIPTIVE NOTES (Type of report and inclusive dates)			
Technical Report No. 224 - October 1973			
5. AUTHOR(S) (First name, middle initial, last name)			
Joseph R. Lapointe, Jr.			
6. REPORT DATE		7a. TOTAL NO. OF PAGES	7b. NO. OF REFS
October 1973		130	31
8a. CONTRACT OR GRANT NO.		9a. ORIGINATOR'S REPORT NUMBER(S)	
N000124-67-A-0181-0032		TR 224	
b. PROJECT NO.		9b. OTHER REPORT NO(S) (Any other numbers that may be assigned this report)	
		036040-19-T	
10. DISTRIBUTION STATEMENT			
Approved for public release; distribution unlimited.			
11. SUPPLEMENTARY NOTES		12. SPONSORING MILITARY ACTIVITY	
		Office of Naval Research Department of the Navy Arlington, Virginia 22217	
13. ABSTRACT			
<p>Cyclo-Stationary (CS) processes are those nonstationary processes that appear to be stationary when observed at integral multiples of a basic interval. Wide Sense Cyclo-Stationary (WSCS) processes possess autocorrelation functions and autocorrelation matrices with a cyclic structure for continuous and discrete time respectively. Discrete time WSCS processes normally arise from sampling continuous time WSCS processes. Other sampling schemes such as multiplexing samples from different stationary random processes or multiplexing samples from the sensors of an array also generate random processes with a cyclic structure in the autocorrelation matrix. The optimum detector for the fixed time forced choice detection of discrete time WSCS processes in additive noise is designed according to the likelihood ratio. The detector design is constrained to preserving the cyclic structure of the signal autocorrelation matrix followed by a signal enhancement filter followed by energy detection. The structure of the signal enhancement filter is clearly identifiable with the cyclic structure of the signal autocorrelation matrix. A suboptimum detector is also presented and is the low input signal-to-noise ratio form of the optimum detector. The optimum and suboptimum detector performance is evaluated for a discrete time real zero mean CS Gauss-Markov process in the region $0.01 \leq P_D \leq 0.99$ and $0.01 \leq P_{FA} \leq 0.9$. The optimum and suboptimum Receiver Operating Characteristics (ROC) are binormal in this region. There is little difference between the optimum and suboptimum performance though the suboptimum ROC is more binormal than the optimum ROC.</p>			

KEY WORDS

LINK A

LINK B

LINK C

ROLE

WT

ROLE

WT

ROLE

WT

Signal Detectability
Cyclo-Stationary Processes
Wide Sense Cyclo-Stationary Processes
Suboptimum and optimum detector
Receiving Operating Characteristics

